Period Adding with Symmetry Breaking/Recovering in a Power Inverter with Hysteresis Control

Zhanybai. T. Zhusubaliyev[a], Viktor Avrutin[b], Andrey S. Kucherov[a], Reham Haroun[c], Abdelali El Aroudi[c]

[a]*Department of Computer Science, Dynamics of Non-Smooth Systems International Scientific Laboratory, Southwest State University, 50 Years of October Str., 94, 305040, Kursk, Russia*
[b]*Institute for Systems Theory and Automatic Control, University of Stuttgart, Pfaffenwaldring 9, 70550 Stuttgart, Germany*
[c]*Department d'Enginyeria Electronica, University Rovira I Virgili, Tarragona, Spain*

Abstract

In the present work, we investigate a period adding structure observed in a discontinuous 1D map modeling the behavior of a DC-AC H-bridge inverter with hysteresis control. Supported by experimental measurements from a laboratory prototype, we demonstrate that the structure is partially affected by bistability, so that for some parameter values the system has a single attracting cycle while for other parameter values a pair of attracting cycles of the same period exists. We show that the reason for possible bistability is related to the symmetry of the underlying model. Then, by means of symbolic dynamics, we explain which of the cycles are affected by bistability and which are not.

Keywords: DC-AC inverter, hysteresis control, bifurcation, bistability, period adding, circle map, symmetry breaking, Farey structures.

1. Introduction

Period adding structures, also known as mode-locking structures or Arnol'd tongues, represent one of the most spread bifurcation phenomena which can be observed in a great variety of dynamical systems [1–4]. The distinguishing feature of such structures is frequently put simply as "between periods p and q, there is period $p + q$", where one refers to regions in parameter space associated with cycles of a certain period. Applying this rule ad infinitum, one obtains a countable set of open regions associated with stable cycles and a zero-measure residual set of parameters associated with quasiperiodic dynamics. The Farey summation rule and the resulting devil's staircase are generic properties of rotation numbers of cycles forming these structures.

Another generic property of period adding structures is their self-similarity. Indeed, some specific details on how exactly the regions associated with a given period are organized may differ depending on a specific system under investigation. For example, boundaries of such a region may be associated with different bifurcations (e.g., classical smooth fold bifurcations, border collision bifurcations, including but not limited to fold border collision bifurcations [4]). For this reason, it is widely believed that once the structure of one of the regions forming a period adding structure is identified, the description applies to all other regions, since all of them are organized in the same way. In the present paper, we will discuss an example where this is not completely the case and some of the regions are associated with bistability while the others are not. To the best of our knowledge, such partially-bistability-affected period adding structures have never been reported before.

As for bistability, i.e., the coexistence of two attractors, it may be caused by different effects. In some cases, two bifurcation structures may overlap, so that some attractors belonging to one bifurcation structure coexist with other attractors belonging to the other structure. Here, one may observe, among other effects, the coexistence of stable cycles with arbitrarily different periods. In addition, bistability may appear due to some symmetry of the system's equations of motion. In such cases, one may observe pairs of coexisting cycles of the same period. It has been widely found in various research fields of science and engineering such

Email addresses: Zhanybai@hotmail.com (Zhanybai. T. Zhusubaliyev), Viktor.Avrutin@ist.uni-stuttgart.de (Viktor Avrutin), r3waz73@gmail.com (Andrey S. Kucherov), reham.haroun@urv.cat (Reham Haroun), abdelali.elaroudi@urv.cat (Abdelali El Aroudi)

as in chemistry and biology [5, 6] among others. In the field of power electronics, it has recently been reported for a self-oscillating H-bridge parallel resonant inverter [7] and in a H-bridge wireless power transfer system [8]. Concerning practical applications, this phenomenon is highly undesirable. It increases the grade of uncertainty about the system's dynamics, in particular, because the omnipresent noise can easily translate the system from one basin of attraction to the other one in an unpredictable way. For this reason, it is a relevant task to identify regions associated with bistability. In the present work, we consider a model of a DC-AC power converter (inverter) with hysteresis control. Such systems are widely applied in active filtering [9], AC motor drives [10], uninterruptible power supply (UPS) [11, 12], grid connected PV systems [13], among others (see also[14, 15]). The current hysteresis control in these systems is characterized by fast dynamic response, high accuracy, current limiting capability and easy implementation.

Physical experiments suggest that the considered system exhibits two types of dynamics, namely symmetric and asymmetric solutions. It is natural to assume that – as in many other systems following the so-called "symmetry-breaking/symmetry-recovering scenario" – symmetric solutions are monostable (existing alone), while asymmetric solutions are bistable (existing in pairs). Moreover, it turns out that the parameter space of the considered system is organized by a period adding structure. These observations lead us to the following two questions: First, what are the symmetry properties of the system, causing symmetric and asymmetric solutions to appear? Second, which of the solutions are symmetric and which are asymmetric, and how the symmetry affects the period adding structure. The second question is of significant interest because the resulting partially-bistability-affected period adding structure contradicts the common expectation that all its regions are organized in the same way and asks for an explanation which of the regions forming this structure are bistability-affected and which are not. As discussed below, the answer to the first question is quite simple and follows from the properties of a continuous-time model of the considered system, while the second question is much more sophisticated and leads us to deal with a suitable model in discrete time. Accordingly, the paper is organized as follows:

First, in Sec. 2 we describe the considered power inverter system, the experimental setup (Sec. 2.1) and the measurements showing symmetric and asymmetric orbits (Sec. 2.2). Then, Sec. 3 describes the model of the considered inverter in continuous time. The model is derived in Sec. 3.1 and its properties are discussed in Sec. 3.2. This provides us with an answer to the first question of the paper (why symmetric and asymmetric solutions occur) and demonstrates that asymmetric solutions exist in pairs, leading to bistability. Eventually, Sec. 4 deals with the model of the considered inverter in discrete time. The model given by a suitable first return map is derived in Sec. 4.1 while its properties are briefly summarized in Sec. 4.2. Thereafter, in Sec. 5, we investigate the bifurcation structure occurring in the discrete time model. We demonstrate that the regions in the parameter space associated with several periodic solutions of this map are organized in a period adding structure. Using a symbolic description, we determine the regularities governing the appearance of symmetric and asymmetric cycles. Sec. 6 provides some conclusions and general remarks about the results of the study.

2. Experiments

2.1. Experimental setup

An experimental prototype of an H-bridge-based inverter (Fig. 1) was implemented in the laboratory to obtain some experimental waveforms of the system under study. The schematic circuit diagram of the implemented inverter is shown in Fig. 2. The inverter switches S_1 – S_4 have been implemented using two half-bridge legs ④ with reference APTC60DSKM24T3G from MICROSEMI. Four identical TOROID ⑤ inductors with reference 2300HT-221-V-RC from BOURNS were used. The nominal inductance value of each of them is 230 μH making a total nominal inductance of 920 μH. Two of these inductors were connected in the top side and the two others at the bottom side of the H-bridge inverter output. The inverter was loaded at the other terminals of the inductors by three identical parallel-connected resistances ⑦ of 10 Ω making a total nominal load resistance R of $10/3$ Ω. The inverter is under voltage mode control. Note that current mode control and voltage mode control are equivalent in this inverter since the inductor current is proportional to the output load voltage. The voltage is sensed by using a voltage divider with a gain of about $\beta = 0.2$. The sensed voltage $V_{\rm cs}$ is compared with a sinusoidal reference signal $V_{\rm ref}(t) = V_m \sin(2\pi f_{\rm ref} t$. In all the experiments, the amplitude $V_m = 0.80$ V, the frequency is $f_{\rm ref} = 200$ Hz. The reference signal $V_{\rm ref}(t)$ is provided by a function generator ① Tektronix AFG2021.

The implementation of the hysteresis controller is performed using two comparators (LM319N) and

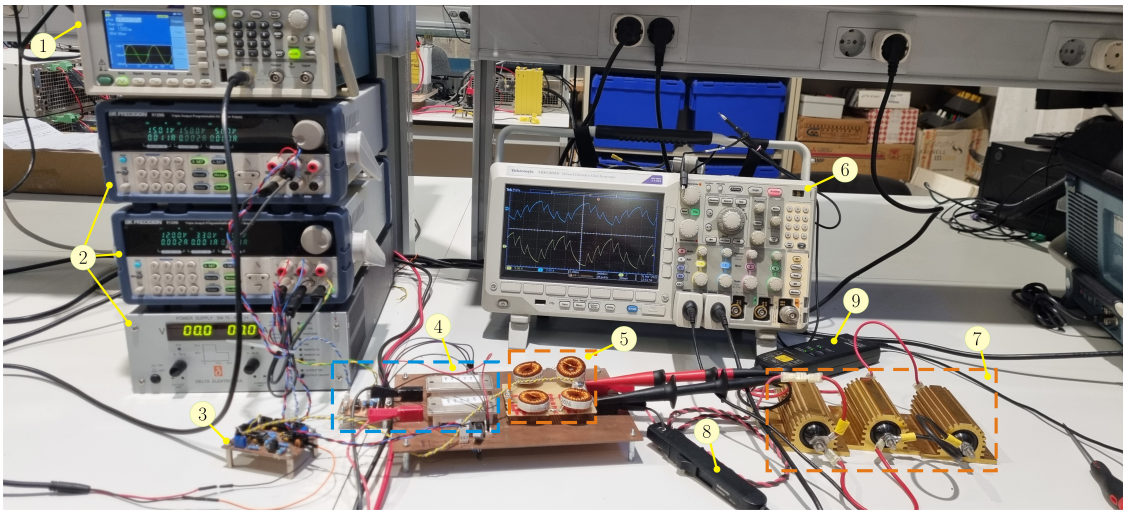

Figure 1: Experimental setup of the considered H-bridge inverter with hysteresis control. ① sine wave $V_{\text{ref}}(t)$ generator; ② two programmable DC power supplies and DC input voltage source; ③ control circuit, ④ two MOSFET power modules containing pairs of switches S_1, S_2 and S_3, S_4; ⑥ digital oscilloscope; ⑤, ⑦ four identical inductors and load resistance (three 10 Ω resistors connected in parallel); ⑧ Current probe and ⑨ differential voltage probe.

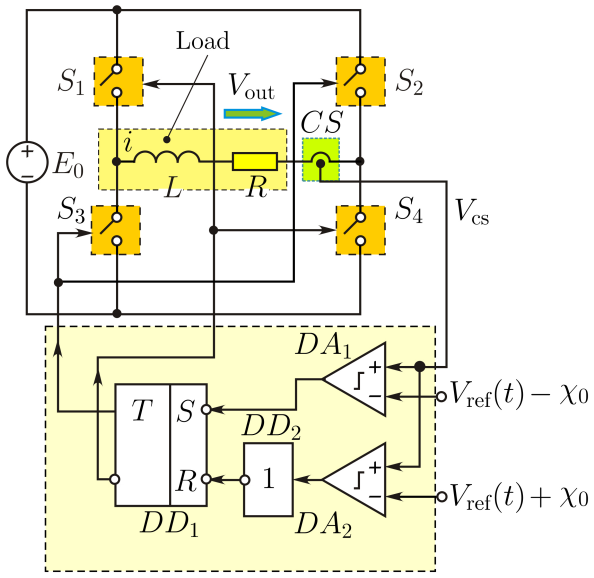

Figure 2: Schematic diagram of the considered H-bridge inverter with hysteresis control.

an S-R flip-flop (CD4027BE). The four MOSFETs (APTC60AN242G) represent the switches $S_1 - S_4$ and are controlled in such a way that when $V_{\text{cs}} < V_{\text{ref}} - \chi_0$, the set (S) signal is triggered turning ON the switches S_1 and S_4 and when $V_{\text{cs}} > V_{\text{ref}} + \chi_0$, the reset (R) signal is triggered turning ON the switches S_2 and S_3. If $V_{\text{ref}} - \chi_0 < V_{\text{cs}} < V_{\text{ref}} + \chi_0$, the state of the flip-flop outputs depends on its condition after its previous switching.

All the measurements are captured using a Tektronix oscilloscope ⑥ MSO 3024. The current probe Tektronix ⑦ TCP0020 was used to measure the inductor current while the load voltage was measured by using the 200 MHz high voltage differential probe ⑧ THDP0200.

2.2. *Experimental results*

Fig. 3 shows two experimentally obtained waveforms of the inductor current and the load voltage for different values of hysteresis width. The desired sinusoidal reference signal is also shown together with the load voltage. Fig. 3(a) corresponds to an unsymmetrical orbit while Fig. 3(b) corresponds to symmetric orbits.

3. Model in continuous time

3.1. *Derivation of the model*

The described inverter system can be modeled by the following differential equation:

$$L\frac{di}{dt} = -R\,i + E_0\,\mathrm{K_F}(\zeta, \eta)$$

where ζ is the error signal given by

$$\zeta = V_m \cos(\omega t) - \beta i(t),$$

i is the load current, and E_0 is the supply voltage.

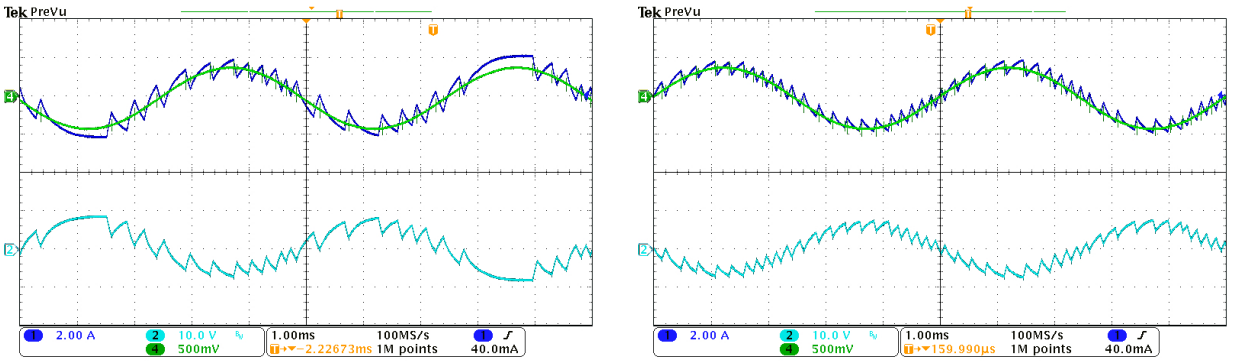

(a) (b)

Figure 3: Experimental waveforms of the H-bridge inverter with hysteresis control. (a) $\chi_0 = 0.15$ V and (b) $\chi_0 = 0.13$ V. Together with the load voltage, the reference sinusoidal signal (amplified by approximately $1/\beta = 5$) is also shown.

Outside the hysteresis zone $[-\chi_0, +\chi_0]$, the switching function $\mathrm{K_F}(\zeta, \eta)$ is given by [16–18]

$$\mathrm{K_F}(\zeta, \eta) = \begin{cases} +1 & \text{if} \quad \zeta > +\chi_0; \\ -1 & \text{if} \quad \zeta < -\chi_0. \end{cases}$$

Inside the hysteresis zone $[-\chi_0, +\chi_0]$, the switching function $\mathrm{K_F}(\zeta, \eta)$ depends on its value η after the previous switching of the relay element [16–18]:

$$\mathrm{K_F}(\zeta, \eta) = \begin{cases} +1 & \text{if} \quad -\chi_0 \leqslant \zeta \leqslant \chi_0 \ \text{ AND } \ \eta = +1; \\ -1 & \text{if} \quad -\chi_0 \leqslant \zeta \leqslant \chi_0 \ \text{ AND } \ \eta = -1. \end{cases}$$

Let us introduce the dimensionless state variable $x = \dfrac{R \cdot i}{E_0}$, the following set of dimensionless parameters

$$q = \frac{V_{\mathrm{ref}}\, R}{\beta E_*}, \quad \chi = \frac{R \chi_0}{\beta E_*}, \quad \Gamma = \frac{E_0}{E_*}$$

and the additional notation

$$q_* = \frac{q}{\Gamma}, \quad \chi_* = \frac{\chi}{\Gamma}, \quad \lambda_* = -\frac{R}{L}, \quad \omega = \frac{2\pi}{T}.$$

Here, q represents the reference voltage, χ and Γ are the hysteresis of the relay element and the DC source voltage, respectively, all normalized with respect to $E_* = 1$ V. In these terms, the model can be rewritten as

$$\frac{dx}{dt} = \lambda_* \left(x - \mathrm{K_F}(\xi, \eta)\right), \tag{1}$$

where

$$\mathrm{K_F}(\xi, \eta) = \begin{cases} +1 \ \text{ if } \ \xi > +\chi_* \ \text{ OR } \\ \qquad (-\chi_* \leqslant \xi \leqslant +\chi_* \ \text{ AND } \ \eta = +1), \\ -1 \ \text{ if } \ \xi < -\chi_* \ \text{ OR } \\ \qquad (-\chi_* \leqslant \xi \leqslant +\chi_* \ \text{ AND } \ \eta = -1), \end{cases}$$
$$\xi = q_* \cos(\omega t) - x(t).$$

Next, let us introduce the dimensionless time variable $\tau = \omega t$. Then, Eq. (1) implies

$$\dot{x} = \frac{dx}{d\tau} = \lambda \left(x - \mathrm{K_F}(x, \eta)\right), \tag{2}$$

where $\lambda = \lambda_*/\omega$, and

$$\mathrm{K_F}(x, \eta) = \begin{cases} +1 \ \text{ if } \ x < q_* \cos\tau - \chi_* \ \text{ OR } \ (\eta = +1 \ \text{ AND } \\ \qquad (q_* \cos\tau - \chi_* \leqslant x \leqslant q_* \cos\tau + \chi_*)\,), \\ -1 \ \text{ if } \ x > q_* \cos\tau + \chi_* \ \text{ OR } \ (\eta = -1 \ \text{ AND } \\ \qquad (q_* \cos\tau - \chi_* \leqslant x \leqslant q_* \cos\tau + \chi_*)\,). \end{cases}$$

In the following, we consider the dynamics of system (2) at the following parameter values: $R = 1.0\ \Omega$; $L = 400\ \mu$H; $V_{\mathrm{ref}} = 4.0$ V; $\beta = 1\ \Omega$; $4 \leqslant E_0 \leqslant 15$ V; $0 < \chi_0 < 4$ V.

3.2. *Properties of the model*

Property 1: *Eq.* (2) *satisfies the following symmetry property:*

$$\mathrm{g}^+(x, \tau) = -\mathrm{g}^-(x(\tau + \pi),\ t + \pi) \tag{3a}$$
$$\mathrm{g}^-(x, \tau) = -\mathrm{g}^+(x(\tau + \pi),\ t + \pi) \tag{3b}$$

in

$$\dot{x} = \mathrm{g}(x, \tau),$$

where

$$\mathrm{g}(x,\tau)=\begin{cases}\mathrm{g}^{+}(x,\tau)=\lambda\,(x(\tau)-1), & \textit{if}\quad \mathrm{K_F}=+1,\\ \mathrm{g}^{-}(x,\tau)=\lambda\,(x(\tau)+1), & \textit{if}\quad \mathrm{K_F}=-1.\end{cases}$$

Let us first prove Eq. (3a). To this end, let

$$x(\tau)=1+(q_*\cos\ \tau_k-\chi_*-1)\mathrm{e}^{(\tau-\tau_k)}$$

be the solution to the equation $\dot{x}=\mathrm{g}(x,\tau)$ with the initial condition $x(\tau_k)=q_*\cos\ \tau_k-\chi_*$ and $\mathrm{K_F}=+1$ between τ_k and τ_{k+1}. Then substituting $x(\tau)$ into $\dot{x}=\mathrm{g}^{+}(x,\tau)=\lambda\,(x(\tau)-1)$ we obtain

$$\begin{aligned}\mathrm{g}^{+}(x,\tau)=&\lambda\ \ (q_*\cos\ \tau_k-\chi_*-1)\,\mathrm{e}^{(\tau-\tau_k)}\\ =&\lambda\cdot\mathrm{e}^{\zeta}\cdot(q_*\cos\ \tau_k-\chi_*-1)\,,\end{aligned}\tag{4}$$

where $\zeta=\tau-\tau_k$. On the other hand,

$$\begin{aligned}\mathrm{g}^{-}(x(\tau+\pi),\tau+\pi)=&\lambda\cdot\mathrm{e}^{\zeta}\cdot(q_*\cos(\tau_k+\pi)+\chi_*+1)\\ =&-\lambda\cdot\mathrm{e}^{\zeta}\cdot(q_*\cos\ \tau_k-\chi_*-1)\,.\end{aligned}\tag{5}$$

The latter equality follows from $\cos(\tau_k+\pi)=-\cos\ \tau_k$. Then, Eq. (3a) follows directly from Eqs. (4), (5). As for Eq. (3b), it can be proven in a similar way.

Eq. (3) implies that if an orbit starting at a point $x=q_*\cos\tau-\chi_*$ at the lower boundary of the hysteresis zone at some phase τ returns to the point x at the same phase τ after some time $2\pi k$, $k>0$, forming in this way a $(2\pi k)$-periodic orbit of system (2), then there is also a periodic orbit of the same period, starting at the point $x'=q_*\cos(\tau+\pi)+\chi_*$ at the upper boundary of the hysteresis zone at the phase $\tau+\pi$. By construction, the two coexisting orbits starting at the points x and x' are symmetric to each other with respect to symmetry (3). In this way, the only possibility for system (2) not to exhibit bistability is that the points x and x' belong to the same periodic orbit, which is then necessarily symmetric to itself with respect to symmetry (3).

Note that symmetry (3) explains why symmetric orbits existing alone and pairs of coexisting asymmetric orbits appear in system (2). However, it does not explain which specific orbits of this system are symmetric or asymmetric, neither any regularities in their appearance. To get this information, it is preferable to use a different kind of description, provided by a discrete time model derived from system (2).

4. Model in discrete time

4.1. Derivation of the map

To obtain a model in discrete time, let us determine a first return mapping from the lower boundary of the hysteresis zone to itself. So, let τ_k and τ'_k be the time instants of the kth switching events occurring at the lower and the upper boundaries of the hysteresis zone, respectively. As $\tau_k<\tau'_k<\tau_{k+1}$, the calculation procedure for the first return map involves two steps, first from the point on the lower boundary

$$x_k=x(\tau_k)=q_*\cos\ \tau_k-\chi_*\tag{6}$$

to the point on the upper boundary

$$x'_k=x(\tau'_k)=q_*\cos\ \tau'_k+\chi_*\tag{7}$$

and then back to the lower boundary:

$$x_{k+1}=x(\tau_{k+1})=q_*\cos\ \tau_{k+1}-\chi_*.\tag{8}$$

Within the time interval $\tau_k<\tau<\tau'_k$, the switching function $\mathrm{K_F}(\varphi,\eta)$ takes the value $+1$. In this case, Eq. (2) is given by

$$\dot{x}=\lambda\,(x-1),\tag{9}$$

and has the solution

$$x(\tau)=1+(x(\tau_k)-1)\mathrm{e}^{\lambda(\tau-\tau_k)}.$$

Then, using the initial condition $x(\tau_k)$ given by Eq. (6) (corresponding to the lower boundary of the hysteresis zone), we obtain

$$x(\tau)=1+(q_*\cos\ \tau_k-\chi_*-1)\mathrm{e}^{\lambda(\tau-\tau_k)}.\tag{10}$$

At the switching time $\tau=\tau'_k$, Eq. (10) implies

$$x(\tau'_k)=1+(q_*\cos\ \tau_k-\chi_*-1)\mathrm{e}^{\lambda(\tau'_k-\tau_k)}.$$

By Eq. (7), it follows

$$q_*\cos\ \tau'_k+\chi_*=1+(q_*\cos\ \tau_k-\chi_*-1)\mathrm{e}^{\lambda(\tau'_k-\tau_k)}\tag{11}$$

Let $z_k^+=\tau'_k-\tau_k$ be the duration of the positive pulse. Then

$$x(\tau'_k)=1+(q_*\cos\ \tau_k-\chi_*-1)\mathrm{e}^{\lambda\,z_k^+},$$

and taking into account Eq. (11), we obtain the following equation with respect to z_k^+:

$$q_*\cos\left(\tau_k+z_k^+\right)+\chi_*=1+(q_*\cos\,\tau_k-\chi_*-1)\mathrm{e}^{\lambda\,z_k^+}.\tag{12}$$

From the solution to this equation, we can find the time instant of the switching event at the upper boundary of the hysteresis zone [18]:

$$\tau'_k=Q^{+}(\tau_k)=\tau_k+z_k^+.\tag{13}$$

In the subsequent time interval $\tau'_k < \tau < \tau_{k+1}$, the switching function $\mathrm{K_F}(\varphi, \eta)$ takes the value -1. Accordingly, Eq. (2) becomes

$$\dot{x} = \lambda\,(x+1), \tag{14}$$

and its solution is given by

$$x(\tau) = -1 + (x'_k + 1)\mathrm{e}^{\lambda(\tau-\tau'_k)}$$

Using the initial condition $x'_k = x(\tau'_k)$ given by Eq. (7) (corresponding to the upper boundary of the hysteresis zone), we obtain

$$x(\tau) = -1 + (q_* \cos\,\tau'_k + \chi_* + 1)\mathrm{e}^{\lambda*(\tau-\tau'_k)}.$$

Then, at the switching time $\tau = \tau_{k+1}$, it follows

$$x_{k+1} = -1 + (q_* \cos\,\tau'_k + \chi_* + 1)\mathrm{e}^{\lambda(\tau_{k+1}-\tau'_k)}.$$

and in this way,

$$q_* \cos\left(\tau'_k + z_k^-\right) - \chi_* = -1 + (q_* \cos\,\tau'_k + \chi_* + 1)\mathrm{e}^{\lambda z_k^-},$$

where $z_k^- = \tau_{k+1} - \tau'_k$. Taking into account Eqs. (7) and (8), we obtain the following equation with respect to z_k^- [18]:

$$q_* \cos\left(\tau'_k + z_k^-\right) - \chi_* = 1 + (q_* \cos\,\tau'_k + \chi_* + 1)\mathrm{e}^{\lambda\, z_k^-}. \tag{15}$$

Similarly to Eq. (13), we conclude [18]

$$\tau_{k+1} = Q^-(\tau'_k) = \tau'_k + z_k^-. \tag{16}$$

Eventually, combining Eqs. (13) and (16), we obtain the following 1D mapping between two subsequent switching times τ_k and τ_{k+1} at the lower boundary of the hysteresis zone [18]:

$$\tau_{k+1} = P(\tau_k) = Q^+ \circ Q^-(\tau_k) = \tau_k + z_k^+ + z_k^-. \tag{17}$$

Actually, the dimensionless time τ can be considered as the phase θ of the external sinusoidal reference signal. Since we consider the phase modulo 2π, i.e., on the circle $0 < \theta < 2\pi$, $\theta = \tau \mod 2\pi$, the two steps described above become [18]

$$\begin{aligned} \theta'_k &= f^+(\theta_k) = Q^+(\theta_k) \mod 2\pi, \\ \theta_{k+1} &= f^-(\theta'_k) = Q^-(\theta'_k) \mod 2\pi. \end{aligned} \tag{18}$$

A successive application of these two mappings leads to the mapping defined on the circle $0 < \theta < 2\pi$ [18]:

$$\theta_{k+1} = F(\theta_k), \quad F(\theta) = f^+ \circ f^-(\theta). \tag{19}$$

4.2. Properties of the map

Depending on its actual parameter values, the function F in map (19) may be continuous or discontinuous. An example of a discontinuous function F is shown in Fig. 4(a). The reason for the appearance of the discontinuities is given by the following property:

Property 2: *The discontinuities of F arise when*

(1) *a solution $x(\tau)$ to Eq. (2) for $\mathrm{K_F} = +1$ starting at the time $\tau = d_1$ on the **lower** boundary $q_* \cos\, d_1 - \chi_*$ of the hysteresis zone becomes tangent to its **upper** boundary $q_* \cos\, d_* + \chi_*$ at the time instant $\tau = d_*$ (see Fig. 4(b)). In this case, the function $F(\theta)$ has a discontinuity at $\theta = d_1$.*

(2) *a solution $x(\tau)$ to Eq. (2) for $\mathrm{K_F} = -1$ starting at the time $\tau = d$ on the **upper** boundary $q_* \cos\, d + \chi_*$ of the hysteresis zone becomes tangent to its **lower** boundary $q_* \cos\, d_{**} - \chi_*$ at the time instant $\tau = d_{**}$ (see Fig. 4(c)). In this case, the function $F(\theta)$ has a discontinuity at $\theta = d_2$ such that the solution $x(\tau)$ to Eq. (2) for $\mathrm{K_F} = +1$ starting at the time $\tau = d_2$ on the lower boundary $q_* \cos\, d_2 - \chi_*$ of the hysteresis zone reaches the upper boundary $q_* \cos\, d + \chi_*$ at the time instant $\tau = d$.*

It is easy to prove that the tangency condition in the case (1) is given by

$$\frac{\partial\varphi}{\partial\tau} + \frac{\partial\varphi}{\partial x} \cdot \mathrm{g}^+(x(\tau),\tau)\Big|_{\tau=d_*} = 0. \tag{20}$$

where

$$\varphi = q_* \cos\,\tau - x(\tau), \quad \mathrm{g}^+(x(\tau),\tau) = \lambda(x(\tau)-1).$$

Since

$$\frac{\partial\varphi}{\partial\tau} = -q_* \sin\,\tau, \quad \frac{\partial\varphi}{\partial x} = -1.,$$

the tangency condition (20) implies

$$-q_* \sin\,\tau - \lambda(x(\tau)-1)\Big|_{\tau=d_*} = 0$$

which means

$$\sin\, d_* + \lambda \cos\, d_* = \frac{\lambda(1-\chi_*)}{q_*}$$

The latter equation implies

$$\cos\,(d_* - \psi) = \frac{\lambda(\Gamma-\chi)}{q\,\sqrt{1+\lambda^2}} \tag{21}$$

where

$$\sin\,\psi = \frac{1}{\sqrt{1+\lambda^2}}, \quad \cos\,\psi = \frac{\lambda}{\sqrt{1+\lambda^2}}$$

Eq. (21) has the solutions

$$d_* = \psi \pm \arccos \frac{\lambda\,(\Gamma - \chi)}{q\sqrt{1+\lambda^2}} + 2\pi\, n, \quad n \in \mathbb{Z}. \tag{22}$$

which exist if and only if

$$-1 \leqslant \frac{\lambda\,(\Gamma - \chi)}{q\sqrt{1+\lambda^2}} \leqslant 1. \tag{23}$$

Since $\lambda < 0$,

$$\psi = \arccos \frac{\lambda}{\sqrt{1+\lambda^2}}.$$

and therefore

$$d_* = \arccos \frac{\lambda}{\sqrt{1+\lambda^2}} + \arccos \frac{\lambda\,(\Gamma - \chi)}{q\sqrt{1+\lambda^2}}. \tag{24}$$

Accordingly, under condition (23), the function F in map (19) has a discontinuity at $\tau = d_1$ (see Fig. 4(a)) where the value d_1 is determined by the equation

$$d_* = Q^+(d_1)$$

and the limiting values $d_{\mathcal{R}}^1$, $d_{\mathcal{L}}^1$ of F at $\tau = d_1$ are determined by

$$d_{\mathcal{R}}^1 = Q^-(d_*),\ d_1 = Q^+ \circ Q^-(d_{\mathcal{L}}^1). \tag{25}$$

(see Fig. 4(b)).

Similarly, in the case (2), the tangency condition implies

$$\sin\, d_{**} + \lambda \cos\, d_{**} = \lambda(\chi_* - 1)/q_*.$$

Solving this equation with respect to d_{**}, we obtain

$$d_{**} = \arccos \frac{\lambda}{\sqrt{1+\lambda^2}} - \arccos \frac{\lambda\,(\chi - \Gamma)}{q\sqrt{1+\lambda^2}}. \tag{26}$$

Similar to the solution to Eq. (24), this solution exists if and only if the condition (23) is satisfied. Then, map (19) has a discontinuity at $\tau = d_2$ (see Fig. 4(a)) where the value d_2 is determined by

$$d_{**} = Q^+ \circ Q^-(d_2).$$

Here, the limiting values $d_{\mathcal{R}}^2$, $d_{\mathcal{L}}^2$ of F at $\tau = d_2$ are determined by the equations

$$d_{\mathcal{R}}^2 = Q^+(d_{**}),\ d_2 = Q^- \circ Q^+(d_{\mathcal{L}}^2). \tag{27}$$

(see Fig. 4(c)).

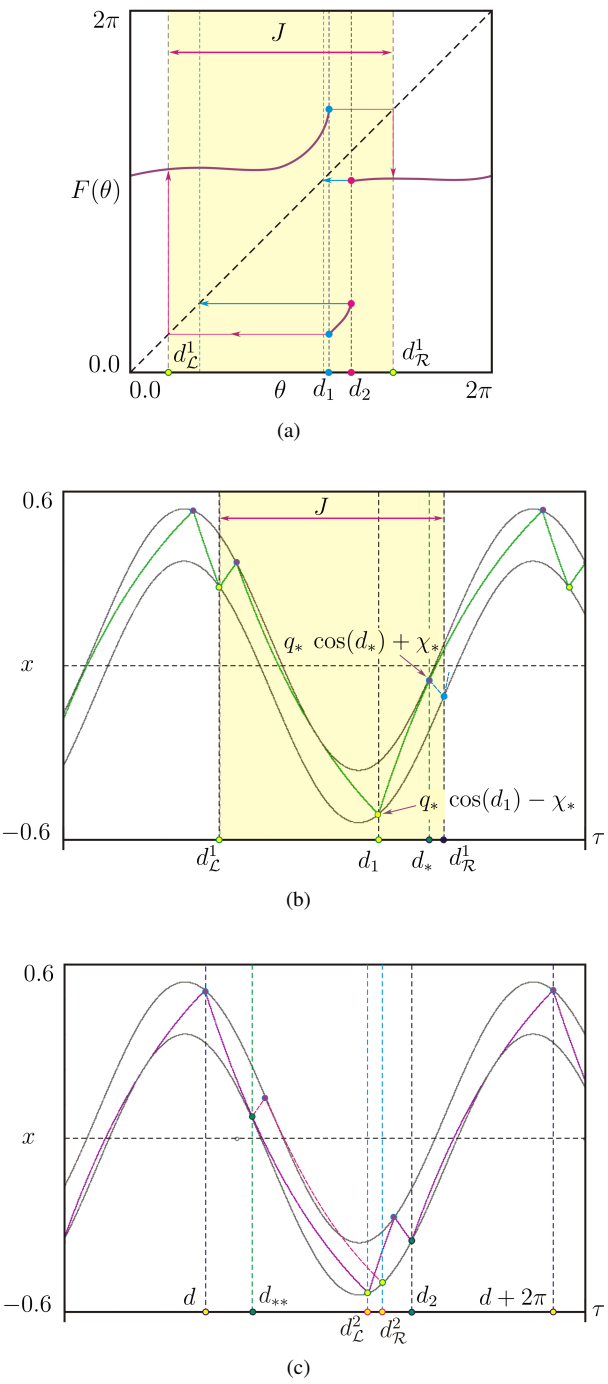

Figure 4: The mechanism leading to the appearance of discontinuities in map (19). The discontinuities d_1 and d_2 shown in (a) correspond to the tangency of an orbit of system (2) with the upper and lower boundaries of the hysteresis zone, as illustrated in (b) and (c), respectively. Additionaly, the points corresponding to the boundaries of the invariant absorbing interval J are indicated.

It follows that the function F in Eq. (19) is continuous if the condition (23) is violated. Accordingly, we can identify the domain

$$\Pi_{\text{circle}} = \left\{ (\Gamma, \chi) \mid \left| \frac{\lambda(\Gamma - \chi)}{q\sqrt{1+\lambda^2}} \right| \geqslant 1 \right\}$$

in the parameter plane where the function F is continuous and monotonously increasing in which case the map (19) is a circle diffeomorphism. For such maps, studied initially by Poincaré himself [19], many theoretical results are proven [20, 21], (see also [22] for a recent overview). In particular, it is known that the maps may exhibit either periodic or quasiperiodic dynamics but no chaos. It is also known that if the dynamics of the map is periodic, cycles of the same period may coexist. It can easily be shown that in the considered parameter range, the boundary of Π_{circle} is given by

$$\delta = \left\{ (\Gamma, \chi) \mid \chi = \Gamma + q\sqrt{1+\lambda^2}\,/\lambda \right\}$$

(see Fig. 6). Beyond the boundary δ, i.e., outside the domain Π_{circle}, the situation is more complicated. In this parameter region, denoted below by Π_{gap}, the map has the following properties:

(A) The map has two discontinuities. Clearly, both discontinuities appear simultaneously as the parameters cross the boundary δ between Π_{circle} and Π_{gap}, which is conform with the symmetry (3).

(B) Asymptotic dynamics of map (19) is confined to the invariant absorbing interval given by

$$J = [\min(d_{\mathcal{R}}^1, d_{\mathcal{R}}^2), \max(d_{\mathcal{L}}^1, d_{\mathcal{L}}^2)].$$

In the considered parameter range, the boundaries of J are determined by the limiting values of the function F at the discontinuity d_1 given by Eq. (25), so that $J = [d_{\mathcal{R}}^1, d_{\mathcal{L}}^1]$ (see Fig. 4(a)). For other parameter values, the limiting values of F at the discontinuity d_2 may be involved in the definition of J as well.

(C) Inside the absorbing interval J, map (19) has so-called gaps, i.e., intervals with no preimages by F inside J. By construction of the function F, these intervals correspond to the inaccessible zones after the points of tangency d_* and d_{**} (see Fig. 4). Clearly, no attractor of map (19) can have a point inside the gaps. The existence of such gaps inside the absorbing interval is a distinguishing property of so-called *gap maps* [23–25], for which several theoretical results are proven. In a rigorous sense, map (19) does not belong to the class of gap maps because these maps are by definition piecewise monotonously increasing while map (19) is not, as demonstrated above. Nevertheless, since map (19) in the considered parameter range is mostly piecewise increasing (the local minima and maxima of

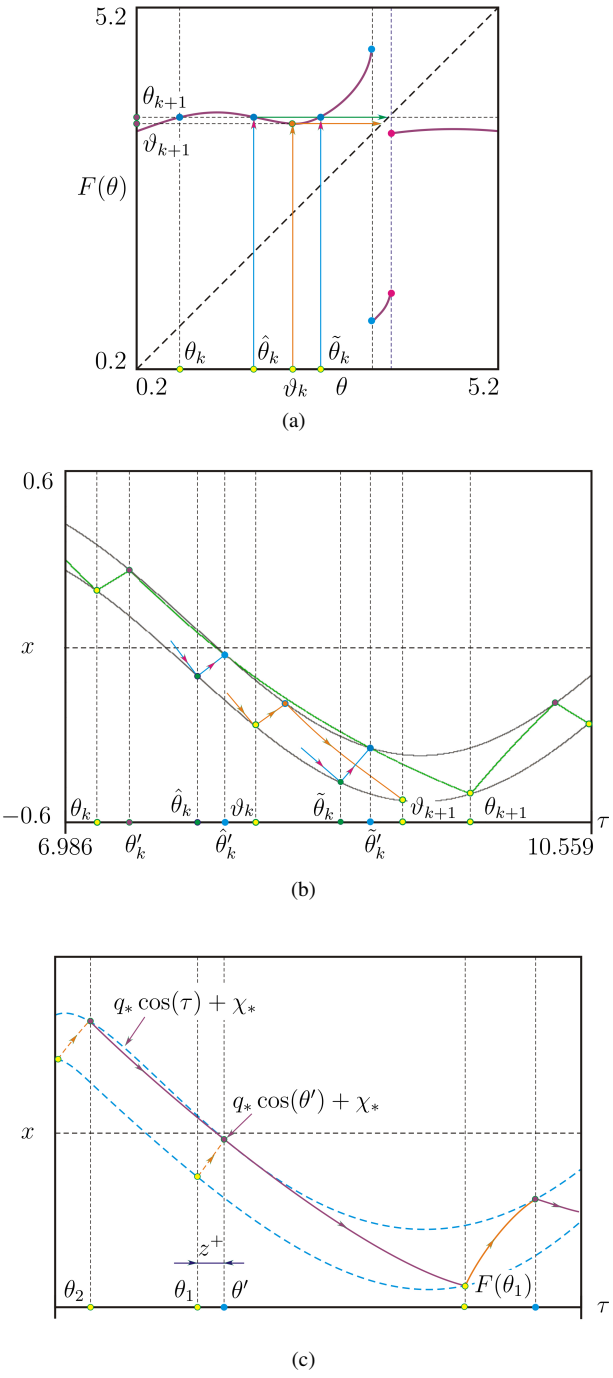

Figure 5: The mechanism leading to the appearance of a local minimum in map (19).

F, if they exist, are not well-developed) and has large gaps inside the absorbing intervals, it can be expected that map (19) may share several properties of gap maps. In particular, a coexistence of cycles of the same period whose periodicity regions in the parameter space are organized in a period-adding structure is a property shared by map (19) and gap maps.

Typically, the function F is piecewise increasing. This is intuitively clear, since if an orbit starting at the lower boundary of the hysteresis zone at the phase θ_k returns to the lower boundary at the phase θ_{k+1}, then it can be expected that an orbit starting at the phase $\theta'_k = \theta_k + \epsilon$, $\epsilon > 0$, will return at the phase $\theta'_{k+1} > \theta_{k+1}$, provided no tangency occurs for orbits starting between θ_k and θ'_k. However, it may also occur that this expectation turns wrong and the function F has a local extremum, as illustrated in Fig. 5(a). As one can see in Fig. 5(b), the orbit of the continuous time system (2) starting at the phase θ_k at the lower boundary of the hysteresis zone returns to this boundary at the phase $\theta_{k+1} = F(\theta_k)$. This orbit reaches the upper boundary at the phase θ'_k, and then – before returning to the lower boundary at θ_{k+1} – crosses the upper boundary at the phases $\hat{\theta}'_k$ and $\tilde{\theta}'_k$. Accordingly, the orbits of system (2) starting at the lower boundary at the phases $\hat{\theta}_k$ and $\tilde{\theta}_k$ as indicated in Fig. 5(b) reach the lower boundary at the same phase θ_{k+1} as the orbit starting at θ_k, i.e., $F(\theta_k) = F(\hat{\theta}_k) = F(\tilde{\theta}_k) = \theta_{k+1}$. Moreover, each orbit starting at the phase ϑ_k with $\hat{\theta}_k < \vartheta < \tilde{\theta}_k$, returns to the lower boundary at the phase $\vartheta_{k+1} < \theta_{k+1}$, so that the function F has a local minimum between $\hat{\theta}_k$ and $\tilde{\theta}_k$.

The described mechanism leads to the following property:

Property 3: *A local extremum of F arises when a solution $x(\tau)$ to Eq. (2) for $K_F = -1$ starting at the time $\tau = \theta_2$ on the* ***upper*** *boundary $q_* \cos\theta_2 + \chi_*$ of the hysteresis zone becomes tangent to the* ***upper*** *boundary $q_* \cos\theta' + \chi_*$ at the time instant $\tau = \theta'$. (see Fig. 5(c)). In this case, the function $F(\theta)$ has a local extremum at $\theta = \theta_1$ such that the solution $x(\tau)$ to Eq. (2) for $K_F = +1$ starting at the time $\tau = \theta_1$ on the lower boundary $q_* \cos\theta_1 - \chi_*$ of the hysteresis zone reaches the upper boundary $q_* \cos\theta' + \chi_*$ at the time instant $\tau = \theta'$.*

For the proof, we refer to Appendix A.

5. Bifurcation structure

5.1. Period adding structure

So far we described the reasons why some of the orbits of system (2) appear in pairs why the others do not. In order to answer the second question of this paper, namely, to find the regularity in their appearance, let us consider the 2D bifurcation structure of map (19) in the parameter plane (Γ, χ) shown in Fig. 6. In this figure, one can observe a typical *period adding* structure. The regions forming this structure are associated with stable cycles of all periods. The organizing properties of this structure are well-known. In particular, let $\mathcal{P}_{p_1/q_1}$ and $\mathcal{P}_{p_2/q_2}$ be two regions in the parameter space associated with cycles O_{p_1/q_1} and O_{p_2/q_2} with periods q_1, q_2 and rotation numbers $\rho_1 = p_1/q_1$ and $\rho_2 = p_2/q_2$. Then, if the numbers ρ_1, ρ_2 are Farey neighbors, i.e., if $|p_1 q_2 - p_2 q_1| = 1$, then between the regions $\mathcal{P}_{p_1/q_1}$ and $\mathcal{P}_{p_2/q_2}$ there exists a region $\mathcal{P}_{p_3/q_3}$ associated with the cycles O_{p_3/q_3} with periods $q_3 = q_1 + q_2$ and rotation numbers $\rho_3 = \rho_1 \oplus \rho_2 = (p_1 + p_2)/(q_1 + q_2)$. Here, $\oplus$ is referred to as the Farey addition, and the number ρ_3 is called a mediant of ρ_1, ρ_2. If the cycles O_{p_1/q_1} and O_{p_2/q_2} are associated with symbolic sequences $\sigma(O_{p_1/q_1})$ and $\sigma(O_{p_2/q_2})$ then the symbolic sequences associated with the cycle O_{p_3/q_3} is given by the concatenation of $\sigma(O_{p_1/q_1})$ and $\sigma(O_{p_2/q_2})$, i.e., $\sigma(O_{p_3/q_3}) = \sigma(O_{p_1/q_1})\,\sigma(O_{p_2/q_2})$. Recall also that a graphical representation of this structure is given by Farey-trees, defined (in the original form) as a directed graph with nodes corresponding to all rational numbers and edges from the nodes n_1, n_2 associated with Farey neighbors ρ_1, ρ_2 to the node ρ_3 corresponding to their mediant ρ_3. Here, the node n_3 is called the child-node of the n_1, n_2, while n_1, n_2 are referred to as the parent-node of n_3. Commonly, the notion of parents and children is adopted for cycles, their associated symbolic sequences and regions in the parameter space as well. A counterpart of the Farey tree defined for symbolic sequences instead of fractions is referred to as a symbolic sequence adding scheme. Here, instead of the Farey addition, a simple concatenation of symbolic sequences is used.

In map (19), the period adding structure in the parameter plane (Γ, χ) originates from an organizing center (codimension-2 point) located in the domain Π_{gap} at the physical boundary of the parameter plane given by $\chi = 0$. The structure continues in the domain Π_{circle}, being formed there by the same regions as in Π_{gap}. The only topological difference between the structures in both domains is related to the bifurcation curves forming the boundaries of the regions. In Π_{circle}, each region

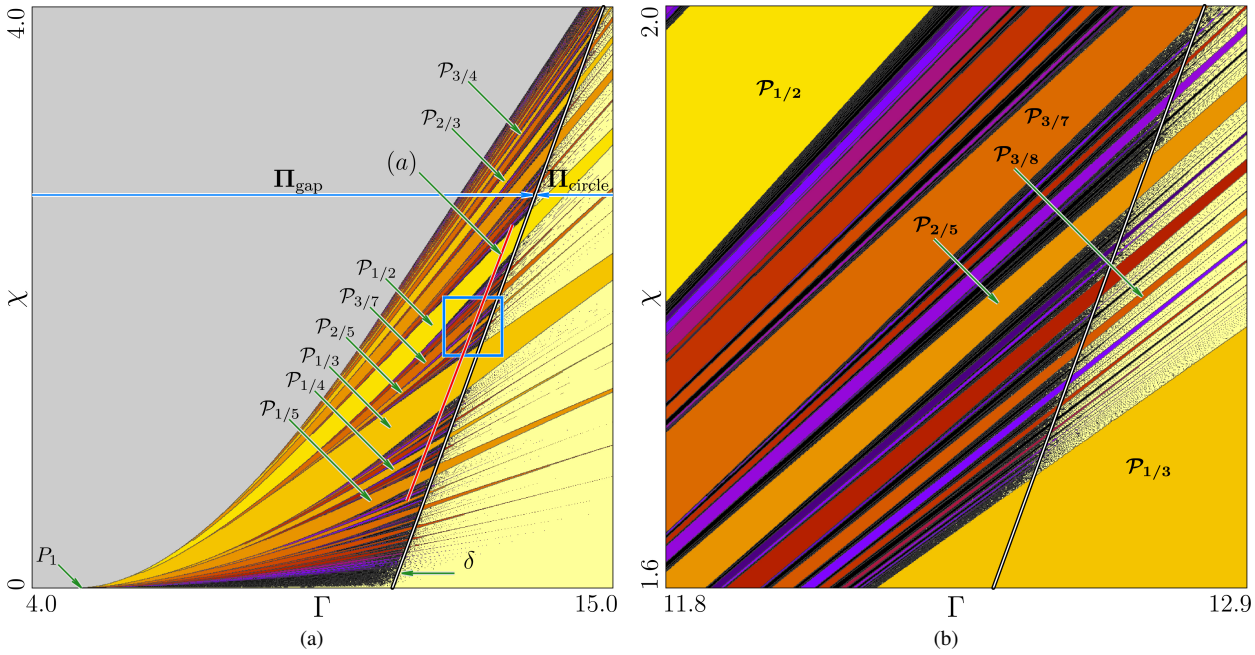

Figure 6: (a) Bifurcation structure in the (Γ,χ) parameter plane of map (19). The bifurcation diagram along the parameter path marked by (a) is shown in Fig. 8. In (b), the rectangle marked in (a) is shown magnified.

is confined by fold bifurcation curves, and as the parameters are moved inside Π_{gap}, the role of boundaries is taken over by border collision bifurcation curves (see Sec. 5.5 for details).

5.2. Which cycles exist in pairs?

However, there is also a difference between bifurcation structures reported in the literature and the bifurcation structure shown in Fig. 6. The first indication of some peculiarity of the latter structure is well-recognizable in Fig. 6(a). Indeed, it can easily be seen in this figure that the regions $\mathcal{P}_{1/q}$, $q \geqslant 3$, where the period q is even, occupy a much smaller area in the parameter space than the surrounding regions $\mathcal{P}_{1/(q-1)}$ and $\mathcal{P}_{1/(q-1)}$ with odd periods. This does not contradict any kind of existing theory, still it is slightly unusual, as in the cases reported in the literature we are aware of, the size of the regions forming a period adding structure typically decreases monotonously with increasing periodicity, regardless the periods being odd or even.

The described property of the period adding structure observed in map (19) is related with the symmetry (3) of the underlying system (2) and the possible bistability resulting from that symmetry. This is intuitively clear for the domain Π_{gap}. Indeed, if there are two coexisting cycles in some region forming the period adding structure in this domain, then a smaller parameter variation is enough to shift a point of a cycle to a discontinuity and to cause a border collision bifurcation than it is necessary if the cycle exists alone.

Note that some cases of bistability-affected period adding structures are reported in the literature, as for example in [26]. However, in the cases we are aware of, all cycles involved in such structures are bistability-affected, since the underlying maps have two absorbing intervals symmetric to each other. This is not the case for map (19) which has a single absorbing interval containing either one or two attracting cycles.

The coexistence of cycles of the same period is also clearly visible in the bifurcation diagram shown in Fig. 8. Here, some of the cycles, as for example $O_{1/3}$, $O_{1/5}$ and $O_{3/7}$, appear alone, while the others, such as $O_{1/2}$, $O_{1/4}$, and $O_{2/5}$, exist in pairs. This leads us directly to the second question of the present paper: what are the regularities in the appearance of bistability in map (19) and hence in the original system (2)? In short, these regularities are determined by the following three properties:

Property 4: *A regions $\mathcal{P}_{1/q}$, $q \geqslant 2$, is associated with a single cycle of map* (19) *with rotation number $1/q$ if q is odd, and with a pair of cycles with rotation number $1/q$ if q is even.*

As an example, Fig. 7(a)-(d) shows the cycles $O_{1/q}$,

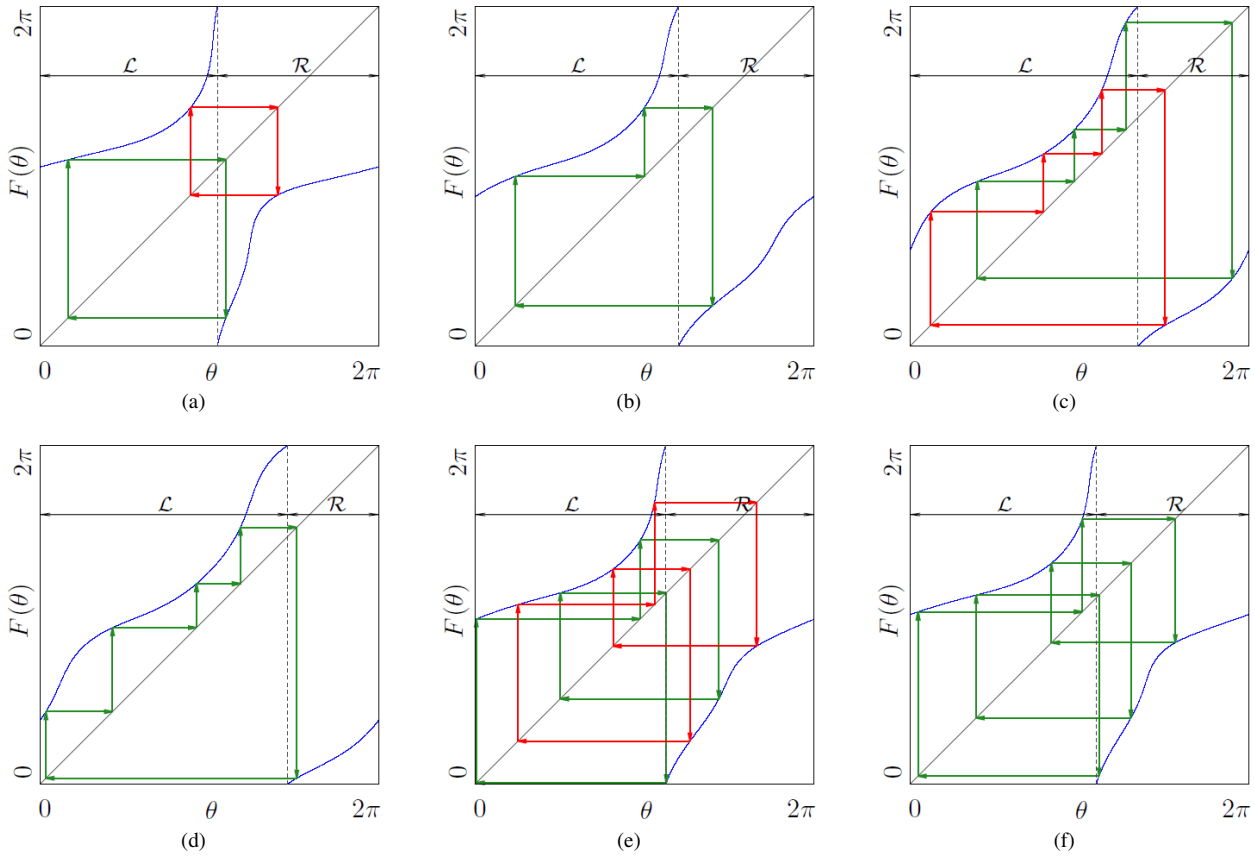

Figure 7: Examples of cycles of map (19) for parameter values in the domain Π_{circ}. (a) Two coexisting 2-cycles $O^{a,b}_{1/2}$ at $\Gamma = 14.8$, $\chi = 3.0$; (b) Single 3-cycle $O_{1/3}$ at $\Gamma = 14.8$, $\chi = 2.174$; (c) Two 4-coexisting cycles $O^{a,b}_{1/4}$ at $\Gamma = 14.8$, $\chi = 1.643$; (d) Single 5-cycle $O_{1/5}$ $\Gamma = 14.8$, $\chi = 1.34$; (e) Two coexisting 5-cycles $O^{a,b}_{2/5}$ at $\Gamma = 14.8$, $\chi = 2.538$; (f) Single 7-cycle $O_{3/7}$ at $\Gamma = 14.8$, $\chi = 2.684$. For the symbolic sequences associated with the presented cycles see Fig. 10.

$q = 2, 3, 4, 5$ for parameter values belonging to the domain Π_{circ}. As one can see, the cycles $O_{1/3}$, $O_{1/5}$ exist alone, being associated with symmetric orbits of system (2), while the cycles $O_{1/2}$, $O_{1/4}$ exist in pairs.

The questions arise which cycles exist in the regions located (in the parameter space) between the regions $\mathcal{P}_{1/q}$, $\mathcal{P}_{1/(q+1)}$ described by Property 4, and which of these cycles are affected by bistability. It can be expected that the rotation numbers of these cycles follow the usual Farey summation rule. However, the question about the associated symbolic sequences is more sophisticated, since usually, a period adding structure can be described by a symbolic sequence adding scheme containing a single symbolic sequence in each node. Therefore, the question is what is contained in a node of a symbolic sequence adding scheme associated with a bistability-affected period adding structure if one or both of its parent-nodes contain two sequences.

Let p_1/q_1, p_2/q_2 be Farey-neighbors and let p_3/q_3 be their mediant $p_3/q_3 = p_1/q_1 \oplus p_2/q_2$. Then the following applies:

Property 5: *Suppose, the region $\mathcal{P}_{p_1/q_1}$ is associated with a single cycle O_{p_1/q_1} and the region $\mathcal{P}_{p_2/q_2}$ is associated with a pair of cycles $O^a_{p_2/q_2}$, $O^b_{p_2/q_2}$. Then the region $\mathcal{P}_{p_3/q_3}$ existing between $\mathcal{P}_{p_1/q_1}$ and $\mathcal{P}_{p_2/q_2}$ is associated with a pair of cycles $O^a_{p_3/q_3}$, $O^b_{p_3/q_3}$ with rotation number p_3/q_3 and the symbolic sequences given by*

$$\sigma(O^a_{p_3/q_3}) = \sigma(O^a_{p_2/q_2})\sigma(O_{p_1/q_1})$$
$$\sigma(O^b_{p_3/q_3}) = \sigma(O_{p_1/q_1})\sigma(O^b_{p_2/q_2})$$

By Property 4, between the region associated with 2-cycles $O^a_{1/2}$, $O^b_{1/2}$ shown in Fig. 7(a) and the region associated with the 2-cycle $O_{1/3}$ shown in Fig. 7(b), there

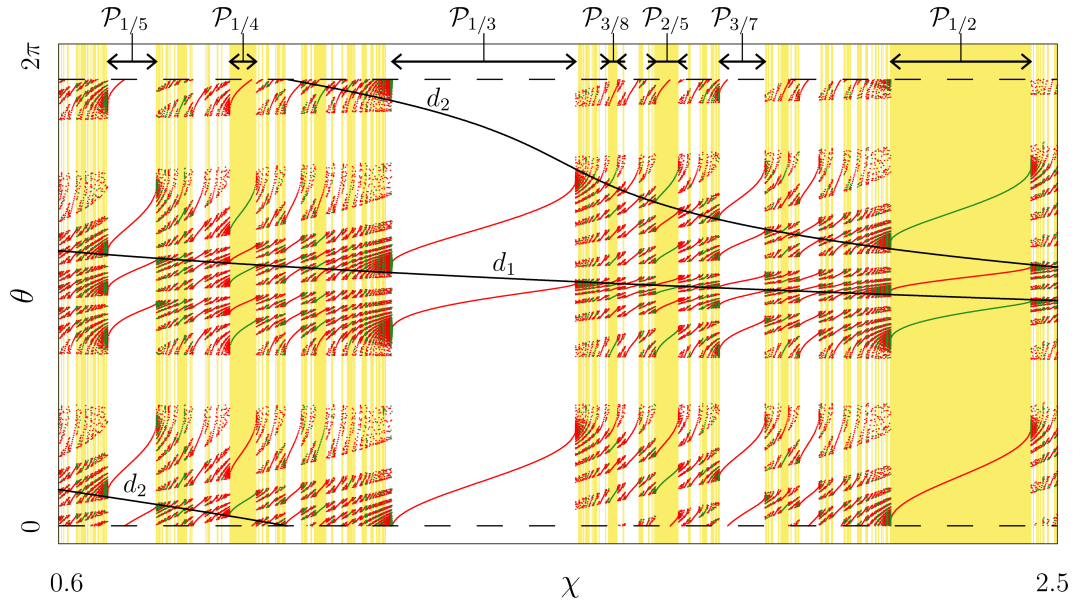

Figure 8: Bifurcation diagram along the parameter path marked in Fig. 6(a). Parameter intervals corresponding to pairs of coexisting cycles are highlighted in yellow. The shapes of the cycles corresponding to some of the marked parameter intervals are shown in Fig. 12, for the associated symbolic sequences see Fig. 13. In addition, the discontinuities d_1 and d_2 of map (19) are indicated.

exists a region associated with a pair of cycles $O^a_{2/5}, O^b_{2/5}$ shown in Fig. 7(e).

Property 6: *Suppose, the region $\mathcal{P}_{p_1/q_1}$ is associated with a pair of cycles $O^a_{p_1/q_1}, O^b_{p_1/q_1}$, while the region $\mathcal{P}_{p_2/q_2}$ is associated with a pair of cycles $O^a_{p_2/q_2}$, $O^b_{p_2/q_2}$. Then the region $\mathcal{P}_{p_3/q_3}$ existing between $\mathcal{P}_{p_1/q_1}$ and $\mathcal{P}_{p_2/q_2}$ is associated with a single cycle O_{p_3/q_3} with rotation number p_3/q_3 and the symbolic sequence*

$$\begin{aligned}\sigma(O_{p_3/q_3}) &= \sigma(O^a_{p_1/q_1})\sigma(O^b_{p_2/q_2}) \\ &\equiv \sigma(O^b_{p_1/q_1})\sigma(O^a_{p_2/q_2})\end{aligned}$$

Applying Properties 5 and 6, we can easily identify which nodes of the Farey structure corresponding to the bistability-affected period adding structure shown in Fig. 6 correspond to pairs of coexisting cycles. In Fig. 9, showing the first layers of this structure, such nodes are indicated. Here, the cycle $O_{1/1}$ in the upper starting node is a fixed point of map (19), while the cycle $O_{0/1}$ in the other starting node has no physical meaning. Indeed, it is clearly visible in Fig. 6 that the regions in the parameter space corresponding to the family of cycles $O_{1/q}$ accumulate for $q \to \infty$ towards the boundary $\chi = 0$. Accordingly, the starting node containing $O_{0/1}$ should correspond to a solution existing for $\chi < 0$ where map (19) is not defined.

The Farey structure shown in Fig. 9 provides also an answer to the question to which extent the period adding structure shown in Fig. 6 is affected by bistability, i.e., which part of all cycles of map (19) exists in pairs, or in other words, which part of all stable cycles of system (2) is asymmetric. Indeed, it can be shown by Properties 5 and 6 that the following apply:

Property 7: *2/3 of all cycles forming the period adding structure in map* (19) *are affected by bistability.*

A proof of this property can be found in Appendix B.

5.3. First symbolic approach

To obtain a more detailed description of the cycles whose stability regions form the period adding structure in map (19), let us introduce their symbolic description. Here, once again, one has to distinguish between the domains Π_{circ} and Π_{gap}.

In the domain Π_{circ}, the simplest way to introduce a symbolic description of the cycles is to consider the map F as a discontinuous map defined on the interval $[0, 2\pi]$ (although on the circle the map is continuous by definition of Π_{circ}). Proceeding in this way, the branches of F can be defined with respect to the point where the function crosses the value 2π. Let us associate the letters $\mathcal{L}$ and $\mathcal{R}$ with the points on the left and on the right of this point, respectively. Then, it can easily be shown that the cycles belonging to the family $O_{1/q}$ have the symbolic description $\sigma(O_{1/q}) = \mathcal{L}^{q-1}\mathcal{R}$. Indeed, it can easily be seen in Fig. 7(a)-(d) that the presented cycles $O_{1/2}$,

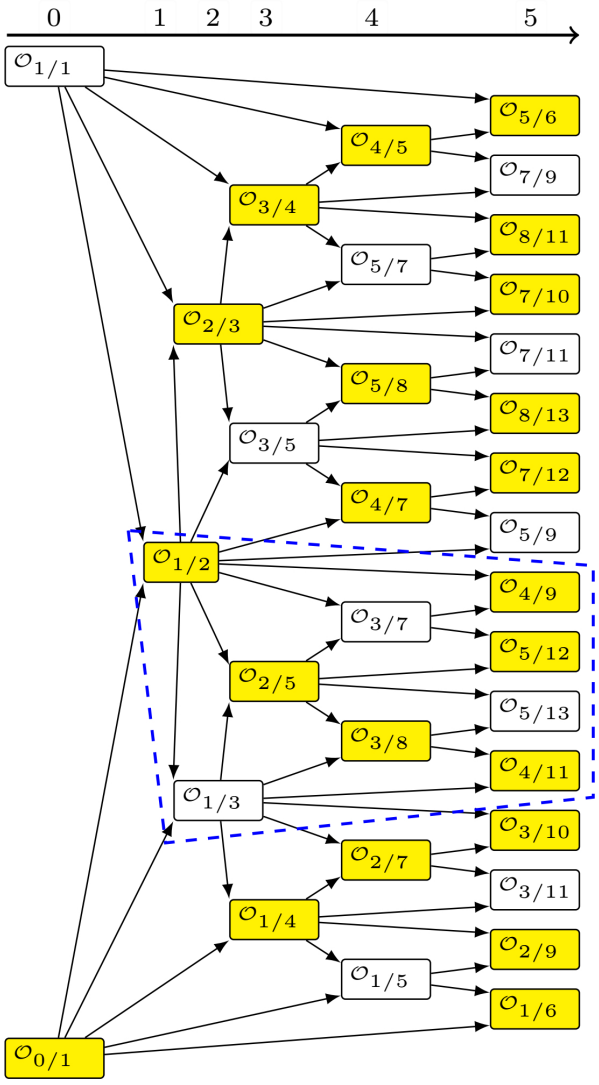

Figure 9: First layers of the symbolic sequence adding scheme corresponding to the period adding structure in map (19). The nodes containing pairs of coexisting cycles are highlighted in yellow. The parts of the symbolic sequence adding schemes corresponding to the part of structure confined by the dashed polygon is shown in Fig. 10 in more detail.

$O_{1/3}$, $O_{1/4}$, and $O_{1/5}$ cycles are associated with symbolic sequences $\mathcal{LR}$, $\mathcal{L}^2\mathcal{R}$, $\mathcal{L}^3\mathcal{R}$, and $\mathcal{L}^4\mathcal{R}$, respectively, regardless they exist in pairs or alone. Similarly, the symbolic description of the cycles from the family $O_{(q-1)/q}$ is $\sigma(O_{(q-1)/q}) = \mathcal{LR}^{q-1}$. For the remaining nodes of the symbolic sequence adding scheme, the symbolic sequences can be obtained by the usual concatenation, so that, for example, the cycles $O_{2/5}$ and $O_{3/7}$ shown in Fig. 7 are associated with symbolic sequences $\mathcal{LRL}^2\mathcal{R}$ and $(\mathcal{LR})^2\mathcal{L}^2\mathcal{R}$. In fact, these cycles belong to a family with the symbolic description $(\mathcal{LR})^k\mathcal{L}^2\mathcal{R}$, $k \geqslant 1$, and it can easily be shown that this family is affected by bistability in the same way as the family $O_{1/q}$ with $\sigma(O_{1/q}) = \mathcal{L}^{q-1}\mathcal{R}$, i.e., bistable cycles and cycles existing alone alternate. This result can also be generalized in terms of *complexity levels* which represent a natural structuring of a symbolic sequence adding scheme, as suggested for the first time by Leonov in [27, 28] (see also [22] for a more detailed description). Following this approach, the starting nodes of a symbolic sequence are said to be of complexity level zero, and then, between two subsequent nodes of complexity level j, $j \geqslant 0$, associated with symbolic sequences σ and ϱ, there exist two infinite families of nodes of complexity level $j+1$ associated with symbolic sequences $\sigma^k\varrho$ and $\sigma\varrho^k$, $k \geqslant 1$. In fact, the overall symbolic sequences adding scheme associated with the period adding structure in map (19) using the symbolic description introduced above is exactly the same as one observes for example in the piecewise linear map [22], as described by Leonov. A part of this symbolic sequence adding scheme corresponding to the dashed polygon marked in Fig. 9 is shown in Fig. 10. As for the bistability in terms of complexity levels, the following applies:

Property 8: *Let σ and ϱ be symbolic sequence associated with nodes of complexity level j, $j \geqslant 0$. Then*
1) If the node associated with σ is bistability-affected, and the node associated with ϱ is not, then the node associated with $\sigma^k\varrho$ is bistability-affected for odd k and not bistability-affected for even k, while the node associated with and $\sigma\varrho^k$ is bistability-affected for all k.
2) If both nodes associated with σ and ϱ are bistability-affected, then both nodes associated with $\sigma^k\varrho$ and $\sigma\varrho^k$ are bistability-affected for odd k and not bistability-affected for even k.

A proof can easily be done by construction. As an example, note that the cycles of complexity level two associated with symbolic sequences $\mathcal{LR}(\mathcal{L}^2\mathcal{R})^k$ exist in pairs for all k, while cycles (of complexity level two as well) associated with symbolic sequences $(\mathcal{LR})^k\mathcal{L}^2\mathcal{R}$ exist in pairs or alone depending on whether k is odd or even (see Fig. 10).

5.4. Second symbolic approach

A disadvantage of the standard symbolic description presented above is that it does not distinguish between coexisting cycles, i.e., coexisting cycles are associated with the same symbolic sequence (see Fig. 7(a),(c),(e)). To obtain a more symbolic description distinguishing

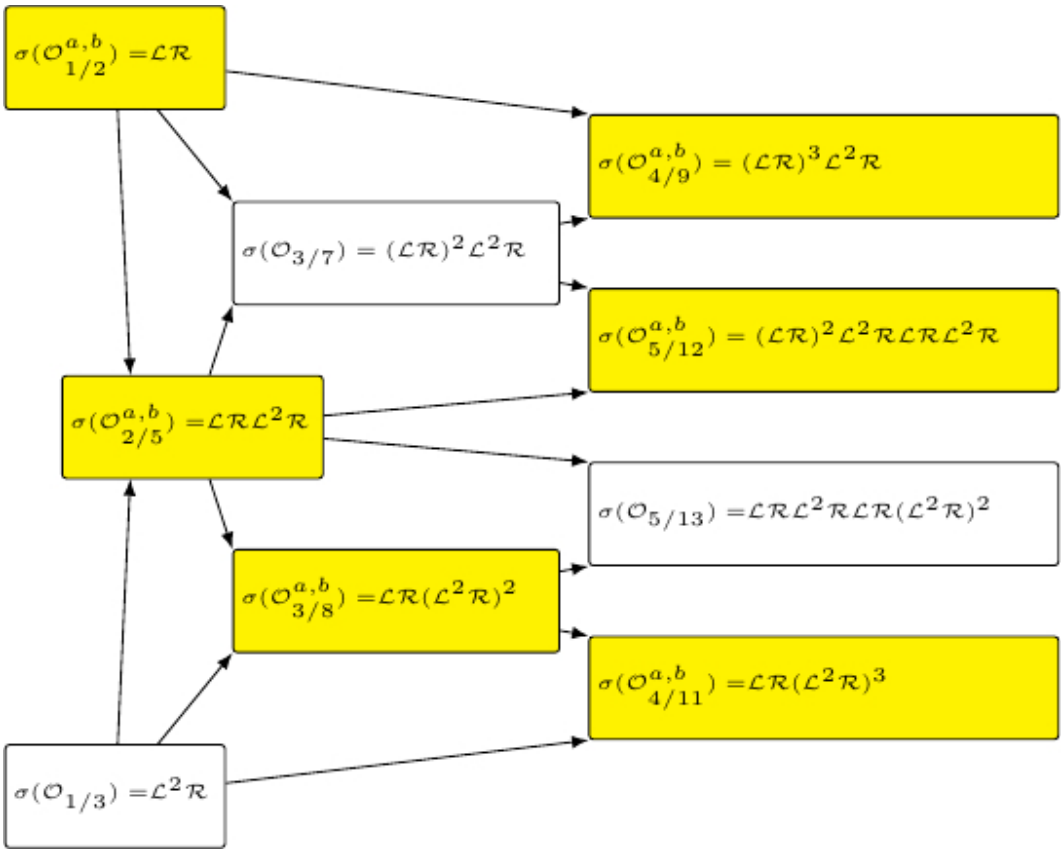

Figure 10: Part of the symbolic sequence adding scheme confined by the dashed polygon in Fig. 9.

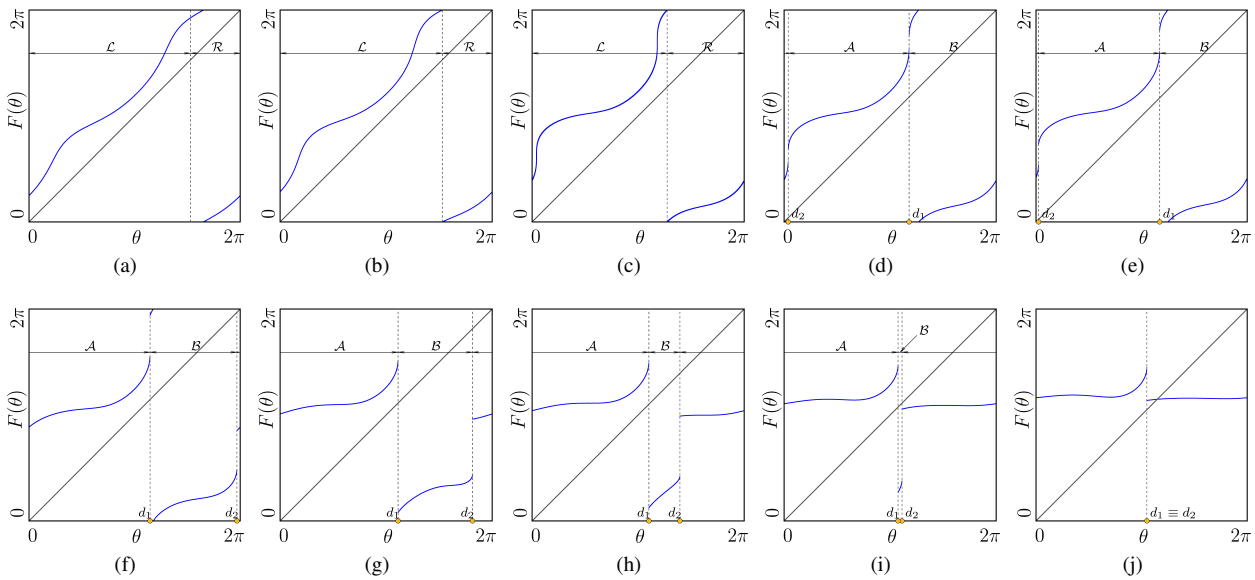

Figure 11: Transformation of the function F under variation of parameters from the domain Π_{circ} to the domain Π_{gap}. (a) $\Gamma = 15.00$, $\chi = 1.0$; (b) $\Gamma = 13.71$, $\chi = 1.0$; (c) $\Gamma = 11.82$, $\chi = 1.0$; (d) $\Gamma = 11.79$, $\chi = 1.0$; (e) $\Gamma = 11.63$, $\chi = 1.0$; (f) $\Gamma = 11.04$, $\chi = 1.0$; (g) $\Gamma = 10.12$, $\chi = 1.0$; (h) $\Gamma = 9.81$, $\chi = 1.0$; (i) $\Gamma = 9.01$, $\chi = 1.0$; (j) $\Gamma = 8,23$, $\chi = 1.0$.

between coexisting cycles, let us consider how the function F changes as the parameters are moved from the domain Π_{circ} into the domain Π_{gap}. An example of this transformation is shown in Fig. 11. As one can see, for parameter values in the domain Π_{circ} far away from its boundary (Fig. 11(a)), the derivative of the function $dF/d\theta$ changes not much over the interval $[0, 2\pi]$ but there are two points in this interval corresponding to local maxima of $dF/d\theta$. As the parameters are moved closer to the boundary δ between Π_{circ} and Π_{gap}, the values of $dF/d\theta$ at these points increase (Fig. 11(b)), and for parameter values approaching δ, these values tend to infinity (Fig. 11(c)). Then, in the domain Π_{gap}, the function becomes discontinuous at these points. Close to the boundary δ, the jumps of the function at these points are relatively small (Fig. 11(d)), and they grow as the parameters are moved farther away from δ (Figs. 11(e) – (h)). Note also that the distance between the discontinuity points d_1 and d_2 changes (Figs. 11(f) – (h)), so that for parameter values approaching the region $\mathcal{P}_{1/1}$ associated with the fixed point of map (19) these points tend to each other (Fig. 11(i)), and in this region, they coincide (Fig. 11(j)).

As a result of the described transformation, the number of branches of the function F considered as a function mapping the interval $[0, 2\pi]$ to itself may vary (cfg. (Figs. 11(d) – (f) where the function has four branches and Figs. 11(g) – (i) where it has only three branches). By contrast, considering this function as a discontinuous function on a circle is significantly simpler. In this way, the function has two points of discontinuity, namely d_1 and d_2, and hence two branches. Let us associate the letter $\mathcal{A}$ with the branch of F located between the points d_1 and d_2, and the letter $\mathcal{B}$ with the branch located between d_2 and d_1. Using this kind of symbolic dynamics, we obtain different symbolic sequences for coexisting cycles.

As an example, let us consider again the cycles of map (19) shown in Fig. 7 for parameter values in the domain Π_{circ}. The same cycles at parameter values in the domain Π_{gap} are presented in Fig. 12. As one can see, the pair of 2-cycles $O^{a,b}_{1/2}$ shown in Fig. 12(a) are associated with different symbolic sequences, namely $\sigma(O^a_{1/2}) = \mathcal{A}^2$ and $\sigma(O^b_{1/2}) = \mathcal{AB}$. Similarly, for the 4-cycles $O^{a,b}_{1/2}$ shown in Fig. 12(c) we obtain $\sigma(O^a_{1/4}) = \mathcal{A}^3\mathcal{B}$ and $\sigma(O^b_{1/4}) = \mathcal{A}^2\mathcal{B}^2$. As for the other cycles from the family $O_{1/q}$ shown Fig. 12(b), (d) it can easily be seen that $\sigma(O_{1/3}) = \mathcal{A}^2\mathcal{B}$ and $\sigma(O_{1/5}) = \mathcal{A}^3\mathcal{B}^2$. These results can be generalized: for a pair of coexisting q-cycle $O_{1/q}$ of complexity level one with even q, the following applies:

$$\begin{aligned} \sigma(O^a_{1/q}) &= \mathcal{A}^{k+1}\mathcal{B}^{k-1} \\ \sigma(O^b_{1/q}) &= \mathcal{A}^k\mathcal{B}^k \end{aligned} \qquad \text{where } k = \frac{q}{2}$$

If q is odd, then for the corresponding cycle we obtain

$$\sigma(O_{1/q}) = \mathcal{A}^{k+1}\mathcal{B}^k \quad \text{where } k = \frac{q-1}{2}$$

As for the second family of cycles of complexity level one, i.e., $O_{(q-1)/q}$, $q \geqslant 2$, here the associated symbolic sequences are given by

$$\begin{aligned} \sigma(O^a_{(q-1)/q}) &= \mathcal{A}^k \\ \sigma(O^b_{(q-1)/q}) &= \mathcal{A}^{k-1}\mathcal{B} \end{aligned} \qquad \text{where } k = q$$

It is worth noticing that the cycles belonging to this family have no or only one letter $\mathcal{B}$ in their symbolic description, while for the first family of cycles of complexity level one, i.e., $O_{1/q}$, $q \geqslant 2$, the number of letters $\mathcal{A}$ and $\mathcal{B}$ is approximately the same. This difference is due to the fact that the regions $\mathcal{P}_{(q-1)/q}$ in the parameter space are located close to the domain of the fixed point $O_{1/1}$ (see Fig. 6). As one can see in Fig. 11(h)–(j), for parameter values approaching the boundary of this domain, the border points d_1, d_2 tend to each other and the length of the branch associated with the letter $\mathcal{B}$ tends to zero. Therefore, the cycles existing in this part of the parameter space are mostly located in the phase interval associated with the latter $\mathcal{A}$.

The symbolic description of the cycles of higher complexity levels can be obtained by concatenation as determined by Properties 5 and 6. As an example, Fig. 13 shows the same part of the resulting symbolic sequence adding scheme as in Fig. 10 (the part corresponding to the polygon marked in Fig. 9). As one can see, the symbolic sequence associated with a pair of 5-cycles $O^{a,b}_{2/5}$ shown in Fig. 12(e) are given by $\sigma(O^a_{1/2}) = \mathcal{A}^4\mathcal{B}$ and $\sigma(O^b_{1/2}) = \mathcal{A}^2\mathcal{BAB}$. It might be surprising that these symbolic sequences do not reflect the symmetry of the underlying cycles of the continuous time system (2). In fact, this follows from the construction of map (19) as a first return map from one of the boundaries of the hysteresis zone to itself. In order to maintain the symmetry of system (2), a different first return map is necessary, defined from the middle of the hysteresis zone to itself.

5.5. Structure of regions

As a final step in the description of the bistability-affected period adding structure in map (19), let us consider the interior composition of specific periodicity regions forming this structure. As already mentioned,

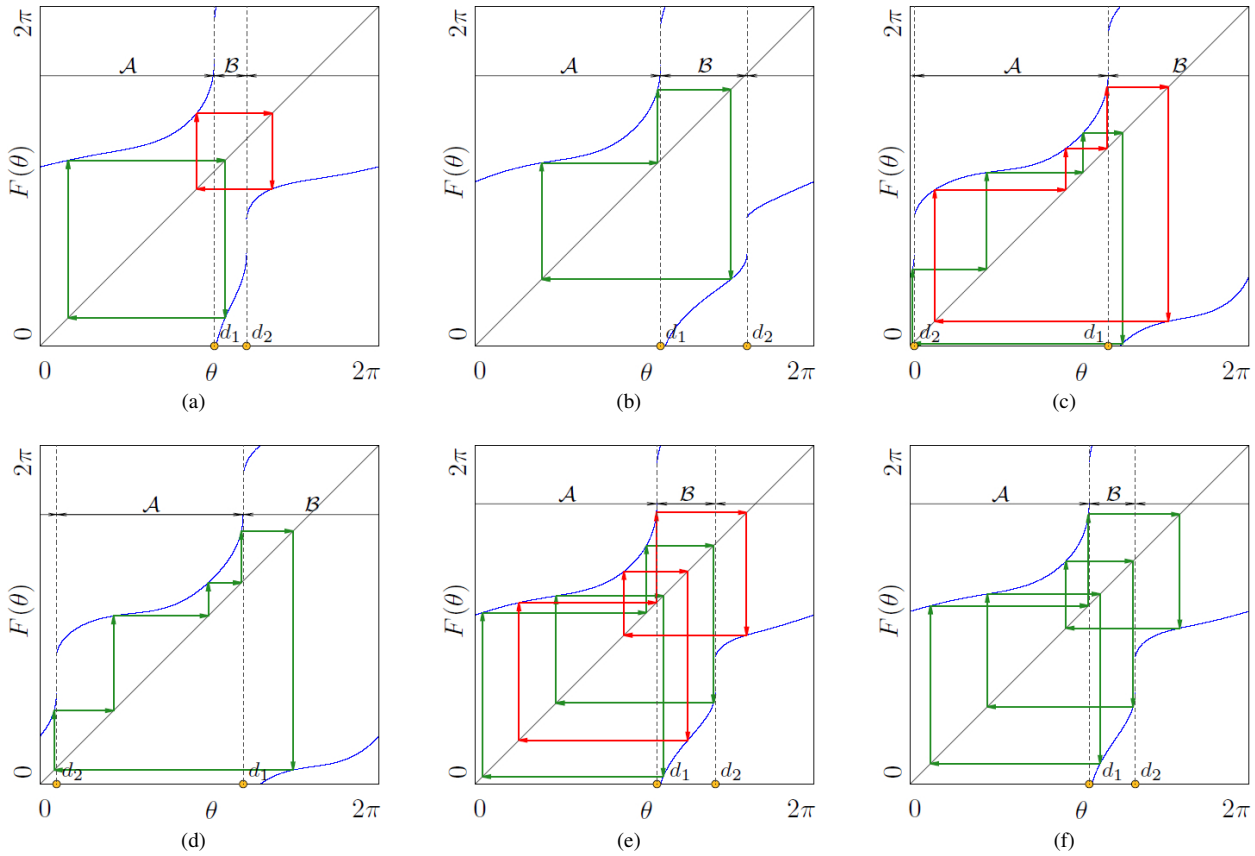

Figure 12: Examples of cycles of map (19) for parameter values in the domain Π_{circ}. (a) Two coexisting 2-cycles $O^{a,b}_{1/2}$ at $\Gamma = 12.85$, $\chi = 2.26$; (b) Single 3-cycle $O_{1/3}$ at $\Gamma = 12.13$, $\chi = 1.577$; (c) Two 4-coexisting cycles $O^{a,b}_{1/4}$ at $\Gamma = 11.47$, $\chi = 0.952$; (d) Single 5-cycle $O_{1/5}$ $\Gamma = 11.29$, $\chi = 0.784$; (e) Two coexisting 5-cycles $O^{a,b}_{2/5}$ at $\Gamma = 12.34$, $\chi = 1.779$; (f) Single 7-cycle $O_{3/7}$ at $\Gamma = 12.22$, $\chi = 1.663$. For the symbolic sequences associated with the presented cycles see Fig. 13.

the boundaries of such regions are associated with border collision bifurcations and with fold bifurcations. For this reason, it is interesting to compare the period adding structure in map (19) with the well-known period adding structure observed for example in the discontinuous piecewise-quadratic map acting as a model of Lorenz-like flows (see [22, 29–31]).

As demonstrated in the cited works, the regions forming this structure are also confined by border collision and fold bifurcation curves. Schematically, the structure of a region associated with cycles O_σ in this map is shown in Fig. 14(b). As one can see, such a region starts at a codimension-2 point A, where the stable cycle O_σ collides with the border simultaneously by two points (from opposite sides). The point A belongs to the gap map domain which contains also a second codimension-2 point, namely a cusp point E from which two fold bifurcation curves issue. Accordingly, in the parameter region between these curves and close to the point E, the map has three cycles of the same period, two stable and one unstable. It is worth noting that among these cycles, the stable ones undergo border collision bifurcations, while the unstable one does not. At the point D, two border collision bifurcation curves intersect (by contrast to the point A, here, not the same cycle collides with the border by two points, but two different cycles) so that bistability in the considered map occurs in the rhomboid-shaped parameter region with the corner points E and D. Note that the point D is located at the boundary of the gap map domain.

In map (19), the structure of a region associated with cycles O_σ is slightly different (see Fig. 14(a)). Similar to the previous case, it begins at the codimension-2 border collision bifurcation point A. However, inside the parameter region confined by two border collision bifurcation curves, there is no cusp point. Instead, there

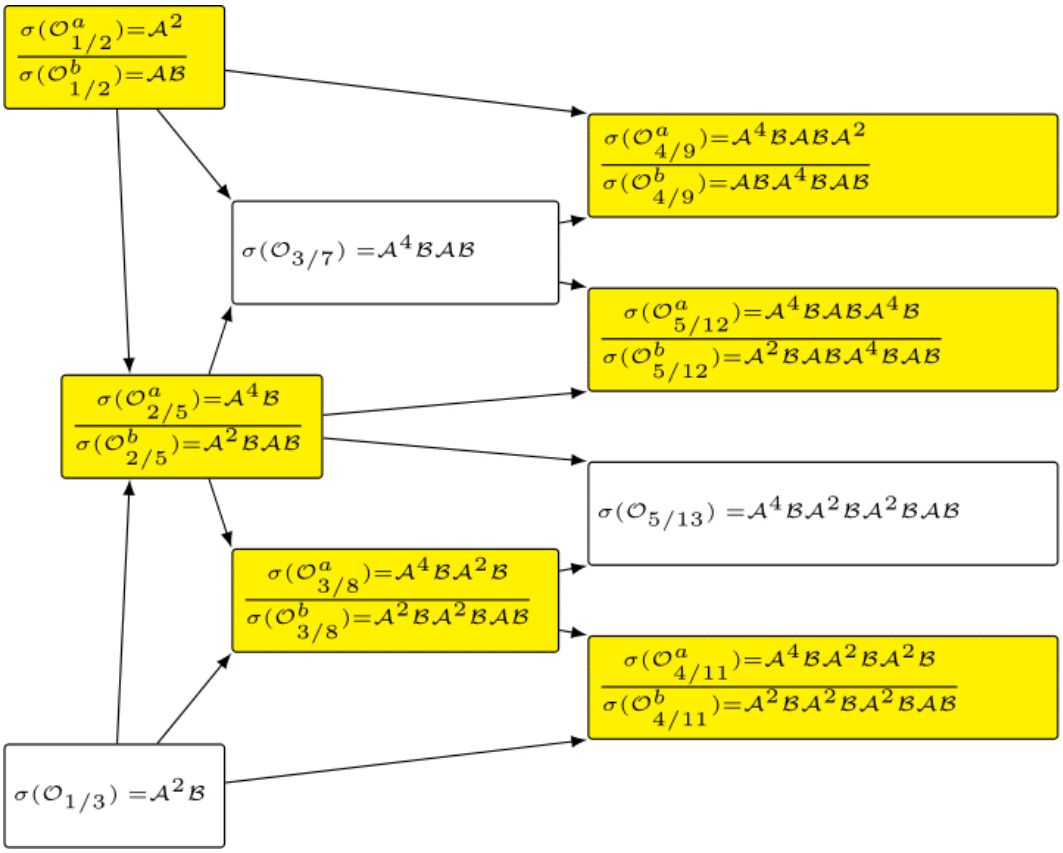

Figure 13: Part of the symbolic sequence adding scheme confined by the dashed polygon in Fig. 9.

are two codimension-2 points B at the boundaries of the region, associated with border collision bifurcations of non-hyperbolic cycles.

From each of these points, a fold bifurcation curve originats, and additionally, the stability of the cycle undergoing border collision bifurcations change. In this way, the point B is connected by border collision bifurcation curves of stable cycles with the codimension-2 point C located at the boundary of the gap map domain. At this point, the border collision bifurcations curves disappear, since beyond the point C the map is in the circle map configuration, and hence has no borders. Instead, a curve associated with 2π-crossing of the cycles originates from this point.

To sum up, there are both similarities and differences between period adding structures in map (19) and in the discontinuous piecewise-quadratic map described in the works cited above. Both structures are formed by regions issuing from organizing centers of the same type. In both cases, the boundaries of the regions close to these organizing centers are given by border collision bifurcation curves, and farther away from the organizing centers, by fold bifurcation curves. However, the origins of these fold bifurcation curves in both maps are different: in the discontinuous piecewise-quadratic map they originate from a cusp point, while in map (19) from codimension-2 points associated with border collision bifurcation of non-hyperbolic cycles. There is also a difference in the stability of cycles undergoing border collisions: in the former case, only stable cycles collide with the border, while in the latter case, both stable and unstable ones do. It is also worth noting that in both maps, the structure starts in the gap map domain. Then, in the discontinuous piecewise-quadratic map, the structure passes through the circle map domain (which is just a curve in the parameter plane commonly considered for this map) and reaches the parameter domain where the map belongs to the class of so-called overlapping maps. In map (19), the circle map domain forms a region in the considered parameter plane. Still, the bifurcation structure in the circle map domain is the same in both maps.

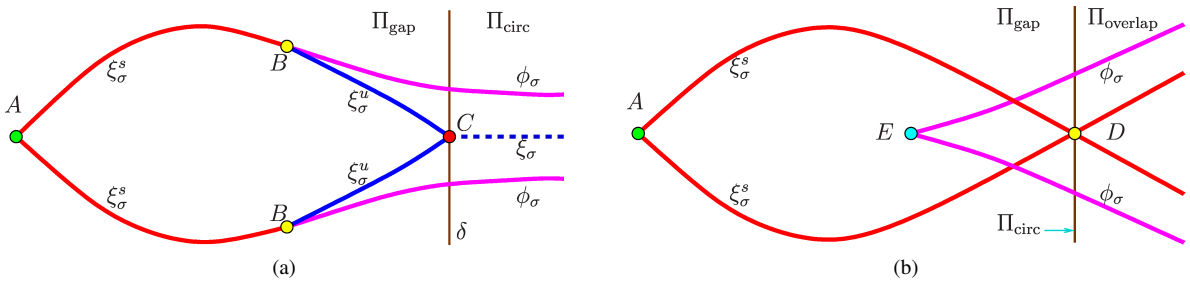

Figure 14: (a) map (19); (b) piecewise quadratic map. ξ^s_σ border collision bifurcation of the stable cycle O_σ; ξ^u_σ border collision bifurcation of the unstable cycle O_σ; φ_σ fold bifurcation; ξ_σ transition over 2π; A organizing center from which the region $\mathcal{P}_\sigma$ originates; B codimension-2 point (border collision and fold taking place simultaneously); C codimension-2 border collision point (two unstable cycles); D codimension-2 border collision point (two stable cycles); E cusp point;

6. Summary

In the present work, we considered periodic dynamics of an H-bridge DC-AC power inverter with hysteresis control. The performed physical experiments show that the considered system may exhibit symmetric and asymmetric waveforms. We have demonstrated that this is due to the symmetry of the equations governing the dynamics of the system. As a consequence, the system has symmetric cycles existing alone and asymmetric cycles which exist in pairs, symmetric to each other. Accordingly, in the latter case, the system exhibits bistability phenomenon.

Moreover, we explained to which extent the considered system is affected by bistability, i.e., which of its cycles are symmetric and which are asymmetric. This has been achieved using a 1D first return map from a boundary of the hysteresis zone to itself. We have shown that if an orbit staring at this boundary becomes tangent to the opposite boundary of the hysteresis zone, this results in a discontinuity in the function governing the dynamics of the first return map. In contrast, if the orbit becomes tangent to the same boundary, it results in a local extremum of the function.

Applying the obtained first return map, it has been shown that the considered 2D parameter space of the system is organized by a period adding structure. Using a symbolic description of this structure (a symbolic sequence adding scheme, similar to well-known Farey trees), we have shown that a cycle is symmetric if both parent nodes of the corresponding node in the symbolic sequence adding scheme are associated with pairs of asymmetric cycles. In contrast, if only one of the parent nodes is associated with a pair of asymmetric cycles, while the other parent node is associated with a single symmetric cycle, then their child node is associated with a pair of asymmetric cycles. Proceeding in this way, we have shown that in total, 2/3 of all cycles of the considered system are bistability-affected.

From a more general perspective, we have investigated the question of how two well-known phenomena widespread in many classes of dynamical systems, namely a symmetry of the equations governing the dynamics and a period adding bifurcation structure, may interact. As reported in the literature, symmetric systems may exhibit bistability because the system has two absorbing intervals symmetric to each other. In such cases, every orbit of the system is bistability-affected. In the case reported in the present work, there is a single absorbing interval, and bistability-affected and -not-affected orbits alternate following the regularities we described.

Acknowledgment

A. El Aroudi and R. Haroun acknowledge the support of the Spanish *Ministerio de Ciencia e Innovación y Universidades* under grant PID2020-120151RB-I00. The work of V. Avrutin was supported by the *German Research Foundation* within the scope of the project "Generic bifurcation structures in piecewise-smooth maps with extremely high number of borders in theory and applications for power converter systems - 2".

References

[1] Ph. Boyland. Bifurcations of circle maps: Arnol'd tongues, bistability and rotation intervals. *Communications in Mathematical Physics*, 106(3):353–381, 1986.

[2] B.-L. Hao. *Elementary symbolic dynamics and chaos in dissipative systems*. World Scientific Publishing, 1989.

[3] A. El Aroudi and R. Leyva. Quasi-periodic route to chaos in a pwm voltage-controlled dc-dc boost converter. *IEEE Trans. Circ. & Sys. I: Regular Papers*, 48(8):967–978, 2001.

[4] Zh. T. Zhusubaliyev, E. A. Soukhoterin, and E. Mosekilde. Quasi-periodicity and border-collision bifurcations in a dc-dc converter with pulsewidth modulation. *IEEE Trans. Circ. & Sys. I: Regular Papers*, 50(8):1047–1057, 2003.

[5] J.E Ferrell Jr. Feedback regulation of opposing enzymes generates robust, all-or-none bistable responses. *Current Biology*, 18(6):2 R244–R245,1–9, 2009.

[6] T. Wilhelm. The smallest chemical reaction system with bistability. *BMC Systems Biology*, 3(90):1–9, 2009.

[7] A. El Aroudi, L. Benadero, E. Ponce, C. Olalla, F. Torres, and L. Martínez-Salamero. Nonlinear dynamic modeling and analysis of self-oscillating H-bridge parallel resonant converter under zero current switching control: Unveiling coexistence of attractors. *IEEE Trans. Circ. & Sys. I: Regular Papers*, 66(4):1657–1667, 2018.

[8] A. El Aroudi, J. Huang, M. S. Al-Numay, and Z. Li. On the coexistence of multiple limit cycles in H-bridge wireless power transfer systems with zero current switching control. *IEEE Trans. Circ. & Sys. I: Regular Papers*, 67(5):1729–1739, 2020.

[9] Y. Kobayashi and H. Funato. Current control method based on hysteresis control suitable for single phase active filter with LC output filter. In *Proc. of 13th Int. Power Electronics and Motion Control Conf.*, pages 479–484. IEEE, 2008.

[10] P. Enjeti, P. D. Ziogas, L. F. Lindsay, and M. H. Rashid. A novel current controlled PWM inverter for variable speed AC drives. In *Proc. of IEEE/IAS Annual Meeting*, pages 235–243. IEEE, 1986.

[11] O. Kukrer, H. Komurcugil, and A. Doganalp. Sliding mode control of single-phase UPS inverters using a three-level hysteresis switching function. In *Proc. of 32nd IEEE Annual Conference on Industrial Electronics (IECON)*, pages 331–335. IEEE, 2006.

[12] S. Saraswathy, K. Punitha, and D. Devaraj. Implementation of current control techniques for uninterruptable power supply. In *Proc. of Int. Conf. on Circuits, Power and Computing Technologies (ICCPCT)*, pages 589–595, 2013.

[13] S. Jena, B.C. Babu, and L. Sahu. Experimental study on adaptive hysteresis current controller for inverter-interfaced 1-Φ grid connected system. In *Proc. of 2011 Annual IEEE India Conference*, pages 1–6. IEEE, 2011.

[14] F. Blaabjerg, editor. *Control of Power Electronic Converters and Systems*, volume 3. Academic Press, 2021.

[15] E. Kabalci, editor. *Multilevel Inverters: Control Methods and Advanced Power Electronic Applications*. Academic Press, 2021.

[16] Zh. T. Zhusubaliyev, E. A. Soukhoterin, V. N. Rudakov, Yu. V. Kolokolov, and E. Mosekilde. Bifurcations and chaotic oscillations in an automatic control relay system with hysteresis. *Int. J. Bif. Chaos*, 11:1193–1231, 2001.

[17] Zh. T. Zhusubaliyev, E. Mosekilde, V. G. Rubanov, and R. A. Nabokov. Multistability and hidden attractors in a relay system with hysteresis. *Physica D*, 306:6–15, 2015.

[18] Zh. T. Zhusubaliyev, V. Avrutin, V. G. Rubanov, and D. A. Bushuev. Complex dynamics of a vibration machine caused by a relay feedback control. *Physica D*, 420:132870, 2021.

[19] H. Poincaré. Sur les courbes définies par les équations différentielles. *J. Math. Pures Appl.*, 4:167–244, 1885.

[20] A. Denjoy. Sur les courbes definies par les equations differentielles a la surface du tore. *J. Math. Pure et Appl.*, 11:333–375, 1932.

[21] V.I. Arnol'd. Small denominators, I : Mappings of the circumference into itself. *Izv. Akad. Nauk SSSR Ser. Mat.*, 25(1):21–86, 1961. (in Russian. See also *Trans. Am. Math. Soc.* 2nd Ser., 46, 213 (1965)).

[22] V. Avrutin, L. Gardini, I. Sushko, and F. Tramontana. *Continuous and Discontinuous Piecewise-Smooth One-dimensional Maps: Invariant Sets and Bifurcation Structures*, volume 95 of *Nonlinear Science, Series A*. World Scientific, 2019.

[23] J. P. Keener. Chaotic behavior in piecewise continuous difference equations. *Trans. Am. Math. Soc.*, 261(2):589–604, 1980.

[24] P. Cvitanovic, B. Shraiman, and B. Söderberg. Scaling laws for mode lockings in circle maps. *Physica Scripta*, 32(4):263–270, 1985.

[25] D. Berry and B.D. Mestel. Wandering interval for Lorenz maps with bounded nonlinearity. *Bull. London Math. Soc*, 23:183–189, 1991.

[26] I. Sushko, F. Tramontana, F. Westerhoff, and V. Avrutin. Symmetry breaking in a bull and bear financial market model. *Chaos, Solitons & Fractals*, 79:57–72, 2015.

[27] N. N. Leonov. On a pointwise mapping of a line into itself. *Radiofisika*, 2(6):942–956, 1959. (in Russian).

[28] N. N. Leonov. On a discontinuous piecewise-linear pointwise mapping of a line into itself. *Radiofisika*, 3(3):496–510, 1960. (in Russian).

[29] I. Procaccia, S. Thomae, and C. Tresser. First-return maps as a unified renormalization scheme for dynamical systems. *Phys. Rev. A*, 35:1884–1900, 1987.

[30] R. Ghrist. Resonant gluing bifurcations. *Int. J. Bif. Chaos*, 10:2141–2160, 2000.

[31] A. J. Homburg. Global aspects of homoclinic bifurcations of vector fields. *American Math. Soc.*, 578, 1996.

[32] Zh. Zhang and F. Comellas. Farey graphs as models for complex networks. *Theoretical Computer Science*, 412(8-10):865–875, 2011.

Appendix A. Proof of Property 3

Fig. 5(c) illustrates a solution $\tilde{x}(\tau)$ to Eq. (2) for $\mathrm{K_F} = -1$ which starts at the time $\tau = \theta_2$ on the upper boundary $q_* \cos\theta_2 + \chi_*$ of the hysteresis zone and is tangent to the upper boundary $q_* \cos\theta' - \chi_*$ at the time instant $\tau = \theta'$.

Since the map F is defined as a first return map from the lower boundary of the hysteresis zone to itself, let us also consider a solution $x(\tau)$ to Eq. (2) for $\mathrm{K_F} = +1$ which starts at the time $\tau = \theta_1$ on the lower boundary $q_* \cos\theta - \chi_*$ and reaches the upper boundary $q_* \cos\theta' - \chi_*$ at the time instant $\tau = \theta'$ which is therefore given by $\theta' = \theta_1 + z^+$. Then, the tangecy condition is given by

$$\frac{\partial\varphi^*}{\partial\tau} + \frac{\partial\varphi^*}{\partial x} \cdot \dot{x}(\tau)\Big|_{\tau=\theta',\ \mathrm{K_F}=-1} = 0 \qquad \text{(A.1)}$$

where

$$\varphi^*(\tau, z) = q_* \cos\tau + \chi_* - x(\tau),$$
$$\dot{x}(\tau)|_{\mathrm{K_F}=-1} = \lambda(x(\tau) + 1)$$

and

$$\frac{\partial\varphi^*}{\partial\tau} = -q_* \sin\tau, \quad \frac{\partial\varphi^*}{\partial x} = -1,$$
$$\dot{x}(\tau) = \lambda(x(\tau) + 1)\Big|_{\tau=\theta'} = \lambda(q_* \cos(\theta + z^+) + \chi_* + 1).$$

Substituting partial derivatives $\frac{\partial\varphi^*}{\partial\tau}$ and $\frac{\partial\varphi^*}{\partial x}$ into Eqs. (A.1), we obtain for $\theta = \theta_1$ the following condition

$$q_* \sin(\theta + z^+) + \lambda\,(q_* \cos(\theta + z^+) + \chi_* + 1) = 0. \quad \text{(A.2)}$$

Let us now demonstrate that condition (A.2) implies the condition of a local extremum of the function $F(\theta) = \theta + z^+(\theta) + z^-(\theta)$. By definition of $F(\theta)$, this condition is given by

$$\frac{dF(\theta)}{d\theta} = 1 + \frac{dz^+(\theta)}{d\theta} + \frac{dz^-(\theta)}{d\theta} = 0. \quad \text{(A.3)}$$

To find the derivative $dz^+/d\theta$, recall that $z^+(\theta)$ is defined implicitly by

$$\varphi^+(z^+, \theta) = 0, \quad \text{(A.4)}$$

so that

$$\frac{\partial\varphi^+}{\partial\theta} + \frac{\partial\varphi^+}{\partial z^+} \cdot \frac{dz^+}{d\theta} = 0$$

and hence,

$$\frac{dz^+(\theta)}{d\theta} = -\frac{\partial\varphi^+/\partial\theta}{\partial\varphi^+/\partial z^+} \quad \text{(A.5)}$$

The derivative $dz^-/d\theta$ can be found similarly. Recall that z^- is defined implicitly by

$$\varphi^-(z^-, z^+, \theta) = 0, \quad \text{(A.6)}$$

were

$$\begin{aligned}\varphi^-(z^-, z^+, \theta) = q_* \cos(\theta + z^+ + z^-) - \chi_* - 1 \\ -(q_* \cos(\theta + z^+) + \chi_* + 1)\, e^{\lambda z^-}.\end{aligned} \quad \text{(A.7)}$$

From Eq. (A.6), it follows directly that

$$\frac{\partial\varphi^-}{\partial\theta} + \frac{\partial\varphi^-}{\partial z^+} \cdot \frac{dz^+}{d\theta} + \frac{\partial\varphi^-}{\partial z^-} \cdot \frac{dz^-}{d\theta} = 0$$

and hence,

$$\frac{dz^-(\theta)}{d\theta} = -\left(\frac{\partial\varphi^-}{\partial\theta} + \frac{\partial\varphi^-}{\partial z^+} \cdot \frac{dz^+}{d\theta}\right) \Big/ \frac{\partial\varphi^-}{\partial z^-} \quad \text{(A.8)}$$

Substituting the expression for $dz^+/d\theta$ given by (A.5) into (A.8), we obtain

$$\frac{dz^-(\theta)}{d\theta} = -\left(\frac{\partial\varphi^-}{\partial\theta} - \frac{\partial\varphi^-}{\partial z^+} \cdot \frac{\partial\varphi^+/\partial\theta}{\partial\varphi^+/\partial z^+}\right) \Big/ \frac{\partial\varphi^-}{\partial z^-} \quad \text{(A.9)}$$

Eventually, combining (A.5) and (A.9), we conclude that condition (A.3) is equivalent to

$$\frac{\partial\varphi^+}{\partial\theta} \cdot \left(\frac{\partial\varphi^-}{\partial z^+} - \frac{\partial\varphi^-}{\partial z^-}\right) + \frac{\partial\varphi^+}{\partial z^+} \cdot \left(\frac{\partial\varphi^-}{\partial z^-} - \frac{\partial\varphi^-}{\partial\theta}\right) = 0. \quad \text{(A.10)}$$

Taking into account that

$$\frac{\partial\varphi^-}{\partial z^+} = \frac{\partial\varphi^-}{\partial\theta},$$

Eq. (A.10) can also be written as

$$\left(\frac{\partial\varphi^+}{\partial z^+} - \frac{\partial\varphi^+}{\partial\theta}\right) \cdot \left(\frac{\partial\varphi^-}{\partial z^-} - \frac{\partial\varphi^-}{\partial\theta}\right) = 0.$$

and hence, condition (A.3) is satisfied (i.e., the $F(\theta)$ has a local extremum) if

$$\frac{\partial\varphi^-}{\partial z^-} - \frac{\partial\varphi^-}{\partial\theta} = 0. \quad \text{(A.11)}$$

Taking into account that

$$\begin{aligned}\frac{\partial\varphi^-}{\partial\theta} &= -q_* \sin(\theta + z^+ + z^-) + q_* \sin(\theta + z^+)\, e^{\lambda z^-}, \\ \frac{\partial\varphi^-}{\partial z^-} &= -q_* \sin(\theta + z^+ + z^-) - \\ &\quad \lambda\,(q_* \cos(\theta + z^+) + \chi_* + 1)\, e^{\lambda z^-}.\end{aligned}$$

Substituting partial derivatives $\frac{\partial\varphi^-}{\partial\theta}$ and $\frac{\partial\varphi^-}{\partial z^-}$ and $\theta = \theta_1$ into Eqs. (A.11), we obtain Eq. (A.2). Therefore, the point $\theta = \theta_1$ is a point of a local extremum of $F(\theta)$.

Appendix B. Proof of Property 7

The proof is based on the correspondence between a Farey structure and a binary tree, see [22, 24, 32]). In this representation, the nodes in a Farey structure can be considered layer-wise: the two starting nodes form its 0th layer, their only common child node forms the 1st layer, and so on. For example, Fig. 9 shows the layers $k = 0, 1, 2, \ldots, 5$ of the overall infinite Farey structure.

Let $p(k)$ be the number of bistability-affected cycles in the kth layer of the considered Farey structure, $k \geqslant 1$, and $q(k)$ the number of cycles existing alone. Properties 5 and 6 imply that

$$\begin{aligned}p(k+1) &= 2q(k) + p(k) \\ q(k+1) &= p(k)\end{aligned} \quad \text{(B.1)}$$

Transforming Eqs. (B.1) into a linear difference equation of the second order

$$p(k+1) = 2p(k-1) + p(k) \quad \text{(B.2)}$$

and solving this equation with the initial conditions $p(1) = 1$ and $p(0) = 0$ (which corresponds to $q(1) = 0$), we obtain

$$p(k) = \frac{1}{3}2^k - \frac{1}{3}(-1)^k \quad \text{(B.3)}$$

Taking into account that the mth layer of a Farey structure, $m \geqslant 1$, contains 2^{m-1} nodes (this follows from the correspondence between a Farey structure and a binary tree), and summing up the number of symmetric cycles in all layers from the first to the mth, we obtain that the ratio of bistability-affected cycles in the overall structure is given by

$$\lim_{m\to\infty} \frac{\sum_{k=1}^{m} p(k)}{\sum_{k=1}^{m} 2^{k-1}} = \frac{1}{3} \lim_{m\to\infty} \frac{\sum_{k=1}^{m} \left(2^k - (-1)^k\right)}{2^m - 1} = \frac{2}{3} \qquad \text{(B.4)}$$

Therefore, the ratio of bistability-affected cycles in the overall structure tends to $2/3$ as $m \to \infty$ which proves the property.